geosciences

MDPI

*Article*

# The Coefficient of Earth Pressure at Rest $K_0$ of Sands up to Very High Stresses

**Maurizio Ziccarelli**

Engineering Department, University of Palermo, Viale delle Scienze Edificio 8, 90128 Palermo, Italy; maurizio.ziccarelli@unipa.it

**Abstract:** The mechanical behaviour of soils subjected to any stress path in which deviatoric stresses are present is heavily characterised by non-linearity, irreversibility and is strongly dependent on the initial state of stress. The latter, for the majority of geotechnical applications, is normally determined by the at-rest earth pressure coefficient $K_0$, even though this state is valid, strictly speaking, for axisymmetric conditions and for zero-lateral deformations only. Many expressions are available in the literature for the determination of this coefficient for cohesive and granular materials both for normal consolidated and over-consolidated conditions. These relations are available for low to medium stress levels. Results of an extensive experimental investigation on two sands of different mineralogy up to very high stress (120 MPa) are reported in the paper. For reach very high vertical stresses, a special oedometer has been realised. In the loading phase (normal consolidated sands), the coefficient $K_{0n}$ depends on the stress level. It passes from values of about 0.8 to values of about 0.45 in the range of effective vertical stress $\sigma'_v$ = 0.5–4 MPa. Subsequently, $K_{0n}$ is about constant and varies between 0.45 to 0.55 up to very high vertical effective stresses (120 MPa). For the sands employed in the tests, Jaki's relation did not lead to reliable results at relatively low pressures, while at high pressures, the same relationship seems to lead to reliable predictions if it refers to the constant volume angle of shear strength. For the over-consolidated sands, $K_{0C}$ strongly depends on the OCR, and for very high values of OCR, $K_{0C}$ could be greater than Rankine's passive coefficient of earth pressure, $K_p$. This result is due to the very locked structure of the sands caused by the grain crushing, with intergranular contact of sutured and sigmoidal, concavo-convex and inter-penetrating type, that confer to the sand a sort of apparent cohesion and make it similar to weak sandstone.

**Keywords:** very high stress level; one dimensional state of strain; coefficient of earth pressure at rest; over-consolidation ratio; sands



**Citation:** Ziccarelli, M. The Coefficient of Earth Pressure at Rest $K_0$ of Sands up to Very High Stresses. *Geosciences* **2024**, *14*, 264. https://doi.org/10.3390/geosciences14100264

Academic Editors: Meng Lu and Fedor Lisetskii

Received: 31 July 2024
Revised: 15 September 2024
Accepted: 4 October 2024
Published: 7 October 2024



## 1. Introduction

The mechanical response of soils is generally non-linear and irreversible starting from very low stress levels [1–3]; therefore, to predict the mechanical behaviour of soils, knowledge of the initial state of stress (or in situ state of stress) is necessary and is of fundamental importance. The initial state of stress represents the starting point against which the variations in effective and total stresses must be evaluated and represents the initial point of any stress path. Furthermore, it strongly affects the mechanical behaviour of soils, and in presence of structure, the soil–structure interaction, and hence also the structural response [4,5]. In natural soil masses, vertical stresses can be determined under non-restrictive hypotheses (i.e., in the case of one-dimensional deformation) through simple equilibrium equations without considering the constitutive model of soil. The horizontal stresses cannot be determined, even in the case of 1D strain, without the knowledge of the stress–strain history or geologic history [6,7] and the constitutive model of soil. Since, in many cases, the stress and deformation events are not known, the stresses can only be determined directly through in situ tests both for rocks as well as for soils [8–14]. The difficulties and the high costs of these latter, especially at great depths, induce, however, to

investigate the factors from which the horizontal stresses depend on and to research, at least for simpler cases, possible relationships between stresses (horizontal and vertical), mechanical properties and the behaviour of soils and rocks. With reference to the one-dimensional state of deformation the horizontal effective stress, $\sigma'_h$ is normally expressed in function of the vertical effective stress $\sigma'_v$ through the coefficient of earth pressure at rest $K_0$:

$$\sigma'_h = K_0 \, \sigma'_v \tag{1}$$

Several studies have been carried out to link the coefficient $K_0$ and the angle of shear strength $\varphi'$ for normal consolidated soil and between $K_0$, $\varphi'$ and the over-consolidation ratio OCR for over-consolidated soils. Some of the classical relationships are reported below.

- For normal consolidated soils:

  Jaky (1944, 1948) [15,16]

$$K_{0n} = \left(1 - \sin \varphi'\right) \frac{1 + \frac{2}{3} \sin \varphi'}{1 + \sin \varphi'} \tag{2}$$

$$K_{0n} = 0.9\left(1 - \sin \varphi'\right) \tag{3}$$

$$K_{0n} = 1 - \sin \varphi' \tag{4}$$

  Hendron (1963) [17]:

$$K_{0n} = \frac{1}{2} \frac{1 + \frac{\sqrt{6}}{8} - 3\frac{\sqrt{6}}{8} \sin \varphi'}{1 + \frac{\sqrt{6}}{8} + 3\frac{\sqrt{6}}{8} \sin \varphi'} \tag{5}$$

  Brooker and Ireland (1965) [6]:

$$K_{0n} = 0.95 - \sin \varphi' \tag{6}$$

  Mesri and Hayat (1993) [18]:

$$K_{0n} = 1 - \sin \varphi'_{cv} \tag{7}$$

  Federico et al. (2008) [19]:

$$K_{0n} = \frac{1 - \sin \frac{2}{3}\varphi'}{1 + \sin \frac{2}{3}\varphi'} \tag{8}$$

- For over-consolidated soils:

  Schmidt (1966, 1967 [20,21]); Alpan (1967) [22]:

$$K_{0C} = K_{0n}(OCR)^m \tag{9}$$

  Wroth (1975) [9].

- For slightly over-consolidated soils (OCR < 5):

$$K_{0C} = (OCR)K_{0n} - \frac{\nu'}{1 - \nu'}(OCR - 1) \tag{10}$$

- For heavily over-consolidated soils (OCR > 5):

$$m\left[\frac{3(1 - K_{0n})}{1 + 2K_{0n}} - \frac{3(1 - K_{0C})}{1 + 2K_{0C}}\right] = \ln\left[\frac{(OCR)(1 + 2K_{0n})}{1 + 2K_{0C}}\right] \tag{11}$$

  Daramola (1980) [23]:

$$K_{0C} = (OCR)K_{0n} - \xi(OCR - 1) \tag{12}$$

Mayne and Kulhawy (1982) [10]:

$$K_{0C} = (1 - \sin \varphi')(OCR)^{\sin \varphi'} \quad (13)$$

Terzaghi, Peck and Mesri (1996) [24].

- For heavily over-consolidated soils that have been subjected to preshearing processes:

$$K_{0n} = (1 - \sin \varphi'_{cv}) \left( \frac{\sigma'_p}{\sigma'_{v0}} \right)^{\sin \varphi'_{cv}} \quad (14)$$

where $\sigma'_p$ and $\sigma'_{v0}$ are the maximum and the actual vertical effective stress respectively.

- For over-consolidated soils of recent deposition and that have not been subjected to aging, preshearing and vibrations:

$$K_{0C} = K_{0n} \left( \frac{\sigma'_p}{\sigma'_{v0}} \right)^{(1-K_{0n})} \quad (15)$$

Parry (2004) [25]:

$$K_{0C} = K_{0n}(OCR)^m \quad (16)$$

in which $m = \varphi'$ is expressed in radians.

The validity of the above relationships has been analysed and verified on the basis of laboratory results at relatively low effective stress levels, and some of them refer to clays. Results available in the literature [17,26–30] and some more recent results of studies, some of which have been conducted in centrifuge [31–37], cannot be considered exhaustive on the topic of the coefficient of earth pressure at rest at high or very high stress levels. In the field of soil mechanics, historically, a lot of research has been focused on the mechanical behaviour of soils at low-medium stress levels. However, many practical geotechnical engineering problems fall into the field of high to very high pressures. In fact, very high earth dams, deep mine shafts and deep tunnels may experience soil pressures up to 10 MPa, while deep well shafts (e.g., shafts and tunnels for storage of nuclear waste) may experience stress levels up to 70 MPa, and soils under the tip of deep-driven foundation piles may experience stress levels up to 350 MPa [38]. Pressures in soils subjected to explosions or projectile impacts can even be much higher. Furthermore, many geological and geophysical applications involve soils and rocks situated very deep under the surface of the earth (a few thousand metres) where extremely high stresses are experienced. In all these problems, stress levels up 100 MPa and even higher are reached. Therefore, understanding the mechanical behaviour of soils subjected to very high pressures, and in particular of granular soils, in which grain crushing can occur, is of fundamental importance for the understanding and the solution of particular geotechnical engineering and geological problems.

Results of a very extensive experimental research performed on sands up to very high stress levels are reported and discussed in the present paper. In particular, the study of the changes of $K_0$ with the vertical effective stress $\sigma'_v$ in the loading and unloading phases are reported, along with the influence of the initial characteristics of sands, such as intrinsic strength and shape of grains, grading and void ratio. The relationship between $K_{0n}$ and the angle of shear strength $\varphi'$ at very high vertical effective stresses and the validity of Jaky's relationship for normal consolidated soils, as well as the link between OCR and $K_{0C}$ for over-consolidated soils, are reported. To understand the behaviour of the wide range of sands present in nature, two particular sands were used. The first was a carbonate sand constituted of soft (not very resistant), fragile and crushable grains, while the second was a quartz sand constituted of very strong and hard grains.

## 2. Definitions of $K_0$

The coefficient of earth pressure at rest $K_0$ has been introduced by Terzaghi (1920) [39] and was defined in different ways [18,24,39–44]. According to some authors $K_0$ is expressed in absolute terms:

$$K_0 = \left.\frac{\sigma'_h}{\sigma'_v}\right|_{\varepsilon_{h=0}} \quad (17)$$

where $\sigma'_v$ and $\sigma'_h$ are the vertical and horizontal effective principal stresses, respectively, for one-dimensional state of strain, in which the only deformation that was not zero was the vertical one ($\varepsilon_v$). The horizontal principal effective stress acts on the vertical planes and is independent of the direction of the plane (axisymmetric condition).

In incremental terms, $K_0$ is defined as follows:

$$\hat{K_0} = \left.\frac{d\sigma'_h}{d\sigma'_v}\right|_{\varepsilon_{h=0}} \quad (18)$$

where $d\sigma'_v$ and $d\sigma'_h$ are the increments of the vertical and horizontal effective principal stress, respectively. For stress paths in the $\sigma'_v$–$\sigma'_h$ plane, the Definition (17) refers to $K_0$ secants, while (18) refers to $K_0$ tangents. Definition (17) does not refer to the initial or reference effective stress state. If the stress paths are not straight, the two definitions are not equivalent.

In the present paper, reference will be made to Definition (17), i.e., in terms of components of the effective stress tensor and not in terms of stress increments, and will be considered as the initial state of stress and strain of the soil (reference state) of the unloaded specimen placed inside the oedometric ring, in which all the components of stress and strain were equal to zero.

## 3. Characteristics of the Sands Used and Samples Preparation Method

Two sands have been used in the experimentation. The first one was a natural carbonate bioclastic sand, namely C sand; the second one was a commercial quartz sand, namely Q sand. C sand was made up almost entirely of small fragments of shells, partly worked out by the action of sea waves; the specific weight $\gamma_s$ was 27 kN/m$^3$. From the optical microscope and the electron microscope (SEM) observations, the particles of the C sand were from angular to subrounded, frequently concave and elongated, as shown in Figures 1 and 2. Some grains presented intragranular pores, Figure 2. The sand was prolongedly immersed into flowing tap water (at least 48 h) to wash away salts from the surface of particles. The mineralogical analysis, performed with an X-ray mass diffractometer, demonstrated that the calcium carbonate was present mainly in the amorphous state and the calcium content is 90%. Small quantities of quartz minerals, K-feldspars, pyroxenes, dolomites and micas were present. The grains of this sand were very soft (not very resistant), fragile and crushable, for which particle breakage was present from very small mean stress levels (a few hundred kPa). Different granulometric fractions were obtained from the natural sand by sieving, as shown in Figure 3. Tests referred to in this paper were carried out on three very close monogranular fractions (b), (d), (e), (g) and (h) and on mixture (f), as shown in Figure 3. Q sand was a pure quartz sand with $\gamma_s$ = 26 kN/m$^3$. The sand particles were sharp-edged or sub-rounded, as shown in Figure 4. The grains of this sand were very strong and hard, and the phenomenon of the grain crushing began at mean stress levels of about 10 MPa. Tests on this sand have been performed on (g) and (e) sands, Figure 3.

Specimens were packaged directly in the special oedometer by lightly compacting the sand (tamping), taking care in applying very low mechanical forces to avoid the possible breakage of any particles in the C sands. For sand Q, this problem was irrelevant considering the intrinsic strength and hardness of the single grains. A thin film of polyethylene terephthalate was placed on the inside surface of the oedometer in order to keep friction at a minimum. The skin friction at the interface between the specimen and the surface of the oedometer was measured by means of vertical strain gauges and was negligible,

confirming the results reported in Yamamuro (1993) [27] and Yamamuro et al. (1996) [30]. The maximum applied effective vertical stress was 120 MPa. The vertical load was applied by means of a hydraulic press with load control. The tests were carried out at almost a constant rate axial deformation of 0.5 mm/min. Displacements of the sand have been measured by conventional millesimal micrometres. This type of measurement does not permit us to investigate the very small and the small strain range. Test duration varied in the range 2–4 h. After testing, all the specimens were removed from the oedometer and sieved. Conventional incremental loading tests were also carried out with maximum applied vertical stress up to 19.5 MPa; the results of these tests are not discussed here.


**Figure 1.** Carbonate sand C. Optical microscope photo of initial sand 0.25 < d < 0.42 mm.

(**a**) (**b**) (**c**)

**Figure 2.** Carbonate sand C. Scanning electron microscope (SEM) photos at different scales. (**a**) Sand 0.84 < d < 1.18 mm, (**b**,**c**) sand 0.42 < d < 0.60 mm. Intragranular pores are visible.

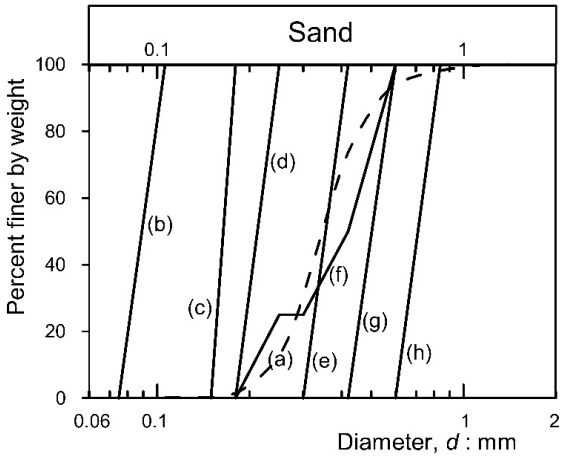


**Figure 3.** Initial grading of the sands utilized in the experimentation. (a) Natural C sand; (b) 0.075 < d < 0.106 mm; (c) 0.15 < d < 0.18 mm; (d) 0.18 < d < 0.25 mm; (e) 0.30 < d < 0.42 mm; (g) 0.42 < d < 0.60 mm; (h) 0.60 < d < 0.84 mm. The sand (f) was composed by 25% (in weight) of sand with 0.18 < d < 0.25 mm, 25% with 0.30 < d < 0.42 mm and 50% with 0.42 < d < 0.60 mm. Tests on Q sand have been performed on (e) and (g) sands, while tests on C sand have been carried out on all the sands.

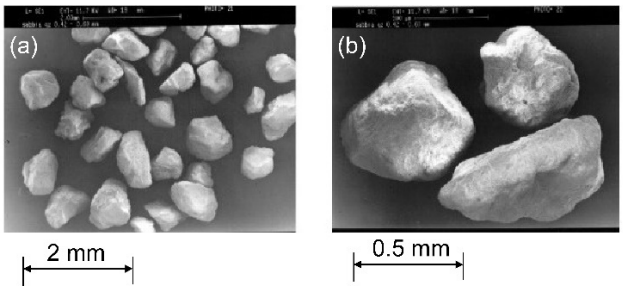


**Figure 4.** (**a**,**b**) Quartz sand Q (0.42 < d < 0.60 mm). Scanning electron microscope (SEM) photos at different scales.

## 4. The Special Oedometer

The experimental dispositive employed for performed the tests was a special very stiff oedometer that was realised from a single block of steel. The scheme of the oedometer is represented in Figure 5. This oedometer made it possible to carry out tests on specimens of heights from 10 to 40 mm. In the range of stresses employed for tests, the oedometer presented linear elastic behaviour. The external lateral area of the oedometer was instrumented with strain gauges for measuring the circumferential strain $\varepsilon_\theta$ and hence for evaluating the horizontal (radial) stress $\sigma'_h$. Monoaxial BHM (Hottinger) strain gauges were installed, category LY11 6/350, with a grid of length of 6 mm and width of 2.9 mm and with nominal resistance of 350 Ohm, gauge factor k of 2 and thermal expansion coefficient $\alpha$ for application on steel of $10.8 \times 10^{-6}$/K. The strain gauges were localised on 2 circumferences at the Weathstone half-bridge as represented in Figure 5. A similar technique to measure $K_0$ was used by Yamamuro (1993) [27] and Castellanza and Nova (2004) [45]. The two circumferences have been chosen in order to have two strain gauges (strain gauges 1 and 2, Figure 5) on the median plane of the specimen in the initial configuration (initial height of the specimen $h_0$ = 20 mm) and two strain gauges on the final one (strain gauges 3 and 4, Figure 5), providing for a representative settlement of 8 mm (final height of the specimen $h_f$ = 12 mm). This value of the final height of the specimen was lower than the minimum one measured with the tests ($h_{f,min}$ = 13.04 mm, settlement of 6.98 mm, test 7, sand C, 0.60 < d < 0.84 mm, $e_0$ = 1.12; see Table 1 in which principal characteristics and results of the tests performed are summarised) and was chosen on the basis of preliminary tests carried out before instrumenting the oedometer.

Through knowledge of the circumferential deformation $\varepsilon_\theta$, the stress $\sigma'_h$ that induces the same $\varepsilon_\theta$ has been determined, in the hypothesis of constant $\sigma'_h$ acting on the ring of the oedometer for a height $h_s$ (Figure 6) corresponding to the measured axial deformations $\varepsilon_a$ and hence to the current height of the specimen.

Given the geometry of the special oedometer realised and the presence of the steel base plate, the available closed-form solutions [46–49] cannot be applied. The link between the average circumferential deformation (average on the two circumferences on which the 4 strain gauges are located) $(\varepsilon_\theta)^*$ induced by a pressure $(\sigma'_h)^*$ = 1 MPa, acting on a height $h_s$ (Figure 6), varying in a field larger than the field representing the possible heights of the specimens actually recorded (initial eight $h_0$ = 20 mm, $h_{min}$ = 12 mm), was determined numerically by the finite element method. The calculation scheme used is represented in Figure 6; the scheme was axisymmetric, and the constitutive model of the steel was linear elastic. The values of Young's modulus (E = 206,000 MPa) and Poisson's ratio ($\nu$ = 0.3) of the steel of the oedometer have been verified by carrying out preliminary tests with measurement of the circumferential deformations using pressurized oil inside the cylinder. Once the pressure of the fluid inside the cylinder was known, a finite element model was built, and the deformations at the points located in correspondence with the electrical strain gauges were determined. The differences between calculated deformations, for the values of the elastic parameters E and $\nu$ reported above, and measured deformations were found to be less than 2%. The results obtained can be considered largely satisfactory considering the simplifications that were introduced in the transition from the real scheme

to the calculation model. It was not possible to construct a relation between the measured pressure and deformations in the strain gauges because the loading area was not the same (in presence of the specimen, the height of the loading area ranged from 12 to 20 mm and was positioned as represented in Figures 5 and 6), and it was not possible to isolate the loaded area in the presence of the sand specimen only. The circumferential deformations were obtained as the average values of those calculated in the Gaussian points located in correspondence of the points where the strain gauges were actually positioned in the real oedometer. Other details were reported in Ziccarelli (1999) [50]. Figure 7 shows the relationship between the calculated mean circumferential deformation $(\varepsilon_\theta)^*$ and the height $h_s$ of the load area, for $(\sigma'_h)^* = 1$ MPa.

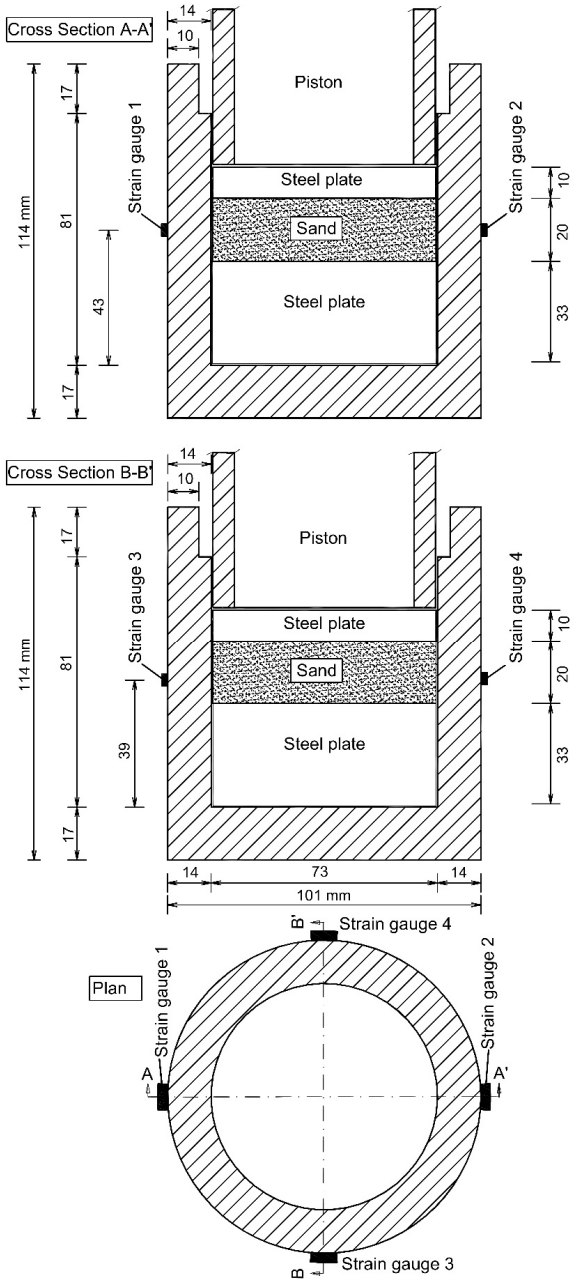


**Figure 5.** Scheme of the special oedometer utilised for the experimentation. The oedometer was equipped with strain gauges to measure circumferential strains. Measurements in mm.

**Table 1.** Principal characteristics and some principal results of the tests performed.

| Test | Sand | Initial Composition d (mm) | $\sigma'_{v,max}$ (MPa) | $e_0$ | $\rho_{max}$ (mm) | $\varepsilon_{a,max}$ ($\times 10^{-2}$) | $\varepsilon_{r,max}$ ($\times 10^{-5}$) | $\varepsilon_{r,max}/\varepsilon_{a,max}$ ($\times 10^{-3}$) | $\nu'$ | $K_0^{(1)}$ | $K_0^{(2)}$ | $K_0^{(*)}$ | $\hat{K}_0^{(*)}$ | a | b | m | β | ξ |
|---|---|---|---|---|---|---|---|---|---|---|---|---|---|---|---|---|---|---|
| 1 | C | 0.30 < d < 0.42 | 80 | 0.64 | 4.80 | 24 | 29.7 | 1.16 | 0.253 | 0.82 | 0.74 | 0.52 | 0.51 | 0.48 | 0.60 | 1.24 | 0.494 | 0.339 |
| 2 | C | 0.30 < d < 0.42 | 80 | 0.77 | 4.84 | 24.2 | 29.7 | 1.16 | 0.275 | 0.83 | 0.76 | 0.62 | 0.54 | 0.49 | 0.58 | 1.34 | 0.450 | 0.379 |
| 3 | C | 0.30 < d < 0.42 | 80 | 0.91 | 5.60 | 28 | 18.7 | 0.58 | 0.250 | 0.95 | 0.64 | 0.51 | 0.50 | 0.47 | 0.60 | 1.25 | 0.495 | 0.334 |
| 4 | C | 0.42 < d < 0.60 | 80 | 0.66 | 4.89 | 24.3 | 30.9 | 1.13 | 0.262 | 0.64 | 0.60 | 0.54 | 0.54 | 0.49 | 0.59 | 1.30 | 0.477 | 0.354 |
| 5 | C | 0.42 < d < 0.60 | 80 | 0.89 | 5.87 | 29.35 | 28.9 | 0.85 | 0.266 | 0.88 | 0.56 | 0.56 | 0.52 | 0.51 | 0.59 | 1.23 | 0.468 | 0.362 |
| 6 | C | 0.42 < d < 0.60 | 80 | 0.77 | 5.18 | 25.9 | 28.0 | 0.94 | 0.254 | 0.65 | 0.60 | 0.51 | 0.50 | 0.46 | 0.59 | 1.26 | 0.493 | 0.340 |
| 7 | C | 0.60 < d < 0.84 | 80 | 1.12 | 6.98 | 34.9 | 27.7 | 0.79 | 0.277 | 0.77 | 0.63 | 0.53 | 0.53 | 0.48 | 0.52 | 1.45 | 0.466 | 0.383 |
| 8 | C | 0.60 < d < 0.84 | 80 | 0.85 | 6.72 | 33.6 | 27.4 | 0.78 | 0.267 | 0.91 | 0.82 | 0.53 | 0.50 | 0.49 | 0.57 | 1.30 | 0.465 | 0.365 |
| 9 | C | 0.18 < d < 0.25 | 80 | 0.64 | 5.59 | 27.95 | 29.0 | 0.94 | 0.259 | 0.79 | 0.62 | 0.54 | 0.50 | 0.44 | 0.69 | 1.12 | 0.483 | 0.349 |
| 10 | C | 0.18 < d < 0.25 | 80 | 0.88 | 5.47 | 27.35 | 27.4 | 0.89 | 0.248 | 0.69 | 0.59 | 0.51 | 0.51 | 0.46 | 0.46 | 1.20 | 0.504 | 0.330 |
| ″ | ″ | ″ | 80 | ″ | 5.50 | 28.15 | 27.5 | 0.98 | 0.239 | / | / | 0.49 | 0.42 | 0.44 | 0.62 | 1.21 | 0.523 | 0.313 |
| 11 | C | 0.18 < d < 0.25 | 80 | 0.71 | 5.03 | 25.15 | 26.5 | 1.05 | 0.248 | 0.50 | 0.45 | 0.52 | 0.52 | 0.46 | 0.60 | 1.19 | 0.491 | 0.329 |
| ″ | ″ | ″ | 100 | ″ | 5.37 | 26.85 | 26.6 | 1.06 | 0.248 | / | / | 0.50 | 0.55 | 0.49 | 0.60 | 1.14 | 0.493 | 0.330 |
| 12 | C | 0.30 < d < 0.42 | 8.3 | 0.77 | 1.09 | 5.45 | 3.3 | 0.61 | 0.27 | 0.48 | 0.44 | 0.45 | 0.52 | 0.47 | 0.46 | 1.34 | 0.460 | 0.370 |
| ″ | ″ | ″ | 20.1 | ″ | 2.38 | 11.9 | 8.5 | 0.71 | 0.242 | / | / | 0.52 | 0.60 | 0.52 | 0.50 | 1.38 | 0.468 | 0.319 |
| ″ | ″ | ″ | 80.3 | ″ | 5.63 | 28.15 | 25.5 | 0.91 | 0.276 | / | / | 0.47 | 0.49 | 0.43 | 0.63 | 1.22 | 0.618 | 0.382 |
| ″ | ″ | ″ | 100.4 | ″ | 6.15 | 30.75 | 30.4 | 0.99 | 0.240 | / | / | 0.54 | 0.56 | 0.49 | 0.60 | 1.21 | 0.461 | 0.316 |
| 13 | Q | 0.42 < d < 0.60 | 83.2 | 0.77 | 5.00 | 25 | 27.6 | 1.11 | 0.254 | 0.68 | 0.40 | 0.54 | 0.53 | 0.54 | 0.53 | 1.43 | 0.517 | 0.341 |
| ″ | ″ | ″ | 100.4 | ″ | 5.56 | 27.8 | 30.3 | 1.09 | 0.245 | / | / | 0.51 | 0.54 | 0.48 | 0.52 | 1.43 | 0.511 | 0.324 |
| 14 | C | 0.075 < d < 0.106 | 80 | 0.71 | 4.51 | 22.55 | 23.9 | 1.06 | 0.332 | 0.46 | 0.46 | 0.51 | 0.46 | 0.44 | 0.59 | 1.06 | 0.44 | 0.389 |
| ″ | ″ | ″ | ″ | ″ | 4.58 | 22.90 | 24.7 | 1.08 | 0.235 | / | / | 0.44 | 0.40 | 0.43 | 0.59 | 1.05 | 0.530 | 0.307 |
| 15 | Q | 0.30 < d < 0.42 | 80 | 0.71 | 5.38 | 26.9 | 29.8 | 1.11 | 0.289 | 0.59 | 0.40 | 0.57 | 0.55 | 0.55 | 0.48 | 1.46 | 0.427 | 0.402 |
| ″ | ″ | ″ | ″ | ″ | 5.62 | 28.1 | 30.1 | 1.07 | 0.267 | / | / | 0.51 | 0.46 | 0.49 | 0.49 | 1.48 | 0.466 | 0.334 |
| 16 | Q | 0.42 < d < 0.60 | 80 | 0.66 | 4.94 | 24.7 | 27.1 | 1.10 | 0.282 | 0.80 | 0.60 | 0.58 | 0.55 | 0.55 | 0.54 | 1.25 | 0.436 | 0.393 |
| ″ | ″ | ″ | ″ | ″ | 5.02 | 25.1 | 27.5 | 1.09 | 0.265 | / | / | 0.52 | 0.43 | 0.49 | 0.56 | 1.31 | 0.471 | 0.360 |
| ″ | ″ | ″ | ″ | ″ | 5.18 | 25.9 | 28.3 | 1.09 | 0.251 | / | / | 0.50 | 0.41 | 0.47 | 0.57 | 1.31 | 0.500 | 0.333 |

**Table 1.** *Cont.*

| Test | Sand | Initial Composition d (mm) | $\sigma'_{v,max}$ (MPa) | $e_0$ | $\rho_{max}$ (mm) | $\varepsilon_{a,max}$ ($\times 10^{-2}$) | $\varepsilon_{r,max}$ ($\times 10^{-5}$) | $\varepsilon_{r,max}/\varepsilon_{a,max}$ ($\times 10^{-3}$) | $\nu'$ | $K_0^{(1)}$ | $K_0^{(2)}$ | $K_0^{(*)}$ | $\hat{K}_0^{(*)}$ | a | b | m | β | ξ |
|---|---|---|---|---|---|---|---|---|---|---|---|---|---|---|---|---|---|---|
| 17 | C | 0.30 < d < 0.42 | 40 | 0.77 | 3.71 | 18.55 | 16.3 | 0.88 | 0.262 | 0.83 | 0.61 | 0.54 | 0.50 | 0.50 | 0.57 | 1.13 | 0.470 | 0.355 |
| ″ | ″ | ″ | ″ | ″ | 3.85 | 19.25 | 16.4 | 0.85 | 0.249 | ″ | ″ | 0.51 | 0.42 | 0.47 | 0.59 | 1.07 | 0.501 | 0.332 |
| ″ | ″ | ″ | ″ | ″ | 3.93 | 19.65 | 16.5 | 0.84 | 0.241 | ″ | ″ | 0.50 | 0.39 | 0.47 | 0.58 | 1.07 | 0.517 | 0.318 |
| 18 | Q | 0.42 < d < 0.60 | 40 | 0.66 | 2.80 | 14 | 15 | 1.07 | 0.236 | 0.71 | 0.62 | 0.57 | 0.63 | 0.57 | 0.51 | 1.38 | 0.446 | 0.383 |
| ″ | ″ | ″ | ″ | ″ | 3.02 | 15.1 | 15.5 | 1.03 | 0.233 | ″ | ″ | 0.52 | 0.45 | 0.52 | 0.53 | 1.32 | 0.489 | 0.343 |
| ″ | ″ | ″ | ″ | ″ | 3.20 | 16 | 16.1 | 1.01 | 0.277 | ″ | ″ | 0.50 | 0.42 | 0.50 | 0.53 | 1.32 | 0.503 | 0.331 |
| 19 | C | 0.30 < d < 0.42 | 8.6 | 0.77 | 0.95 | 4.75 | 3.8 | 0.80 | 0.230 | 0.90 | 0.63 | 0.52 | 0.54 | 0.53 | 0.58 | 1.05 | 0.540 | 0.229 |
| ″ | ″ | ″ | 20.1 | ″ | 2.05 | 10.25 | 8.8 | 0.86 | 0.245 | ″ | ″ | 0.55 | 0.56 | 0.53 | 0.57 | 1.20 | 0.510 | 0.325 |
| ″ | ″ | ″ | 80 | ″ | 5.00 | 25 | 25.7 | 1.03 | 0.244 | ″ | ″ | 0.49 | 0.47 | 0.45 | 0.59 | 1.21 | 0.513 | 0.322 |
| 20 | C | 0.30 < d < 0.42 | 80 | 0.77 | 5.69 | 28.45 | 30 | 1.05 | 0.292 | 0.91 | 0.76 | 0.59 | 0.54 | 0.53 | 0.57 | 1.39 | 0.415 | 0.413 |
| 21 | C | 0.30 < d < 0.42 | 120 | 0.59 | 5.88 | 28.75 | 45 | 1.56 | 0.294 | 0.69 | 0.55 | 0.57 | 0.54 | 0.47 | 0.68 | 1.11 | 0.411 | 0.417 |
| 22 | C | 0.18 < d < 0.25 | 120 | 0.61 | 5.50 | 27.5 | 43 | 1.56 | 0.266 | 0.64 | 0.45 | 0.52 | 0.50 | 0.44 | 0.66 | 1.13 | 0.469 | 0.361 |
| 23 | C | Mix f (Figure 4) | 80 | 0.58 | 4.66 | 23.3 | 32 | 1.37 | 0.237 | 0.60 | 0.53 | 0.56 | 0.53 | 0.50 | 0.62 | 1.23 | 0.525 | 0.311 |
| 24 | C | Mix f (Figure 4) | 81 | 0.77 | 6.25 | 31.25 | 31 | 0.99 | 0.319 | 0.75 | 0.74 | 0.61 | 0.57 | 0.52 | 0.58 | 1.21 | 0.374 | 0.456 |
| 25 | C | Mix f (Figure 4) | 80 | 0.69 | 5.90 | 29.5 | 30 | 1.02 | 0.282 | 0.65 | 0.61 | 0.57 | 0.54 | 0.50 | 0.62 | 1.30 | 0.437 | 0.392 |

Legend: $\sigma'_{v,max}$: maximum vertical effective stress reached in the test; $e_0$: initial void ratio; $\rho_{max}$: maximum settlement of the specimen; $\varepsilon_{a,max}$: maximum axial deformation; $\varepsilon_{r,max}$: maximum radial deformation; $\nu'$: Poisson's ratio; $K_0^{(1)}$: (n must be deleted) coefficient of earth pressure at rest for $\sigma'_v$ = 0.96 MPa; $K_0^{(2)}$: coefficient of earth pressure at rest for $\sigma'_v$ = 1.96 MPa; $K_{0n}^{(*)}$: coefficient of earth pressure at rest for $\sigma'_v = \sigma'_{v,max}$; $\hat{K}_0^{(*)}$ coefficient of earth pressure at rest for $\sigma'_v = \sigma'_{v,max}$ in differential terms; *a* and *b*: coefficient in the relationships $K_0$-OCR (Schimdt, 1966 and 1967 [20,21]; Alpan, 1967 [22]); *m*: inverse of the slope of the line interpolating experimental points in phase of unloading the plane $(q/p') - \ln(p'/p'_{max})$, Wroth (1972) [8]; β: slope of the line interpolating experimental points in phase of unloading the plane s′–t, Wroth (1975 [9]); $\xi = (1 - \beta)/(1 + \beta)$, Daramola, 1980 [23]; $\nu' = \xi/(1 + \xi)$: Poisson's ratio.

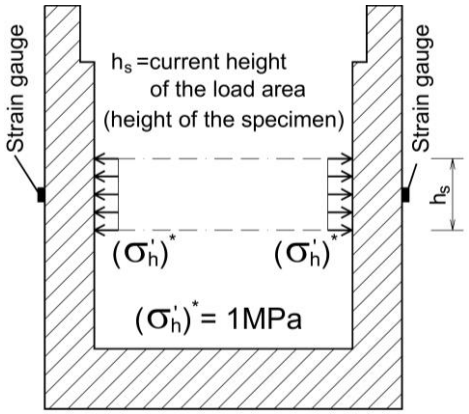


**Figure 6.** Scheme for the determination, by axisymmetric FEM calculation, of the relation between the applied pressure $(\sigma'_h)^* = 1$ MPa (applied on a variable height $h_s$) and the mean circumferential deformation $(\varepsilon_\theta)^*$.

The relation between the mean circumferential strain $(\varepsilon_\theta)^*$ and the height $h_s$ of the applied pressure $(\sigma'_h)^* = 1$ MPa, obtained by FEM calculations, is represented in Figure 7 and is expressed by the following relation:

$$(\varepsilon_\theta)^* = (0.0324 + 0.2587\, h_s)\left(*10^{-6}\right) \tag{19}$$

This relationship was linear in the range of $h_s$ (load height) between 12 and 22 mm and was inclusive of the actual heights measured in the tests, ranging from 13.08 to 20 mm.

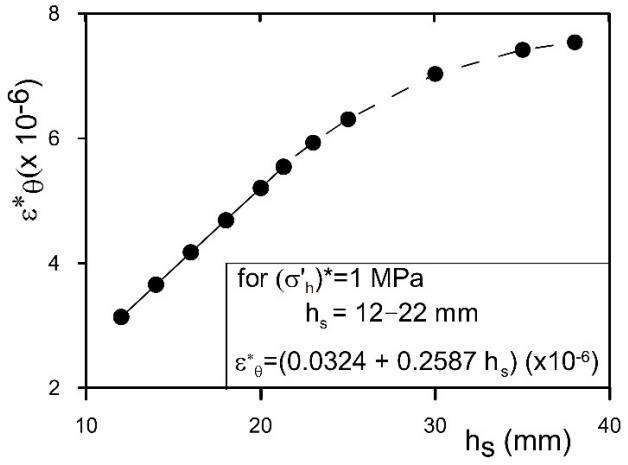


**Figure 7.** Relation between mean circumferential deformation $(\varepsilon_\theta)^*$ and height of the applied pressure $h_s$ (expressed in mm) and for $(\sigma'_h)^* = 1$ MPa. All tests carried out fall within the 12–20 mm range of height $h_s$ of load (see Table 1).

To verify the correctness of the method used, the numerical modelling of the problem under examination was preceded by the modelling of a problem for which the theoretical solution was available; an indefinite cylinder subjected to constant radial pressure was modelled; the results obtained showed differences between the theoretical and the numerical solution that were practically zero or negligible. During the tests, the application of a vertical effective pressure $\sigma'_v$ on the top of the specimen of sand, transmitted by the piston through the upper steel load plate (Figure 8a), induced the state of stress of Figure 8b. The horizontal effective pressure $\sigma'_h$ represents the action of the specimen of the sand, of current thickness $h_s$ (Figure 8c), on the internal annular surface of the oedometer (assuming a constant distribution of $\sigma'_h$). Stress horizontal $\sigma'_h$ was back-calculated as the pressure that induce a circumferential deformation $\varepsilon_\theta$ equal to the mean value of the measured

one $\varepsilon_{\theta m}$ (mean of the 4 measurements in the strain gauges) during the generical phase of the generic test. The relation between the horizontal stress $\sigma'_h$ and the circumferential deformation $\varepsilon_{\theta m}$ is the one reported in Equation (20):

$$\sigma'_h = \frac{\varepsilon_{\theta m}}{(\varepsilon_\theta)^*}(\sigma'_h)^* [\text{MPa}] \quad (20)$$

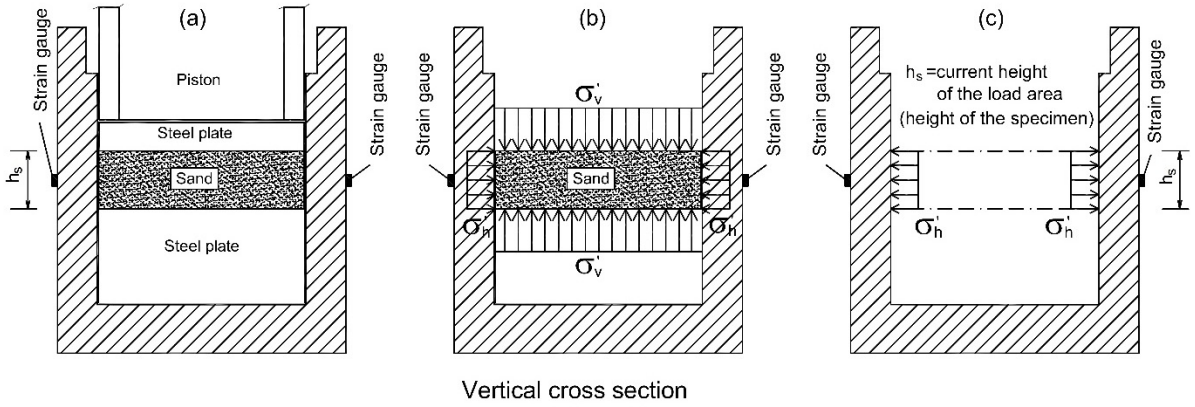


**Figure 8.** Scheme of the current state of tests: (**a**) real situation, (**b**) vertical and horizontal stresses applied on the contour of the specimen, (**c**) scheme for the determination of the horizontal stress $\sigma'_h$ of the special oedometer utilised for the experimentation. Obviously, the horizontal stress $\sigma'_h$ of Figure (**b**) is the same of that of Figure (**c**).

For all the considered thicknesses of the specimen, the radial displacements $\rho_r$ of the internal surface of the oedometer and linked to the value of the circumferential deformation $\varepsilon_{\theta m}$ have been determined by the FEM analysis. The value of $\rho_r$ ranged from $4 \times 10^{-4}$ to $1.11 \times 10^{-3}$ mm for $\sigma'_v$ variable between 6 and 120 MPa. These displacements were of the same order of magnitude of those obtained in the triaxial cell in tests of the $K_0$ type on many other materials (clay, gypsum sand, quartz sand) and at low to medium stress levels [17,27,30,43,51–56]. The radial strain $\varepsilon_r$ is the following:

$$\varepsilon_r = \frac{\rho_r}{r_0} \quad (21)$$

where $\rho_r$ is the mean radial displacement on the contour of the specimen, and $r_0$ (36.5 mm) is the specimen's initial radius.

From the measured circumferential strains (obtained through the strain gauges measurements), the radial ones and the radial displacements have been determined. The increment of radius obtained from the measured circumferential strains was the same of that calculated with the used FEM model.

The radial deformation $\varepsilon_r$, in correspondence of the maximum value of the applied vertical stress of the generic test, ranged from $3.3 \times 10^{-5}$ (test 12, $\sigma'_v$ = 8.3 MPa) to $45 \times 10^{-5}$ (test 21, $\sigma'_v$ = 120 MPa), as shown in Table 1, and was of the same magnitude (0.02%) of that indicated by Okochi and Tatsuoka (1984) [53], Lo and Chu (1991) [57], Cardona et al. (2023) [58] and Park and Santamarina (2023) [59] to satisfy one-dimensional strain conditions. Additionally, Andrawes and El-Sohby (1973) [43] reported that small radial strain deviations from zero would not significantly affect the values of $K_0$. They reported test results indicating that the $K_0$ value changed from 0.38 to 0.37 only for a radial to axial strain ratio much larger than the one measured in the present study. Consequently, the effects of the small radial strains observed in this study can be considered negligible. Furthermore, Lirer et al. (2011) [60] experimentally demonstrated that the influence of the deformability of the oedometer ring on the $K_0$ values was very small and therefore negligible.

The axial strain $\varepsilon_a$ is the following:

$$\varepsilon_a = \frac{\rho_a}{h_0} \tag{22}$$

where $\rho_a$ is the axial displacement of the top of the specimen, and $h_0$ (20 mm) is the specimen's initial thickness. The axial deformation $\varepsilon_a$ ranged from $4.75 \times 10^{-2}$ (test 19: 0.30 < d < 0.42 mm, $\sigma'_v$ = 8.3 MPa, $e_0$ = 0.77) to $34.9 \times 10^{-2}$ (test 7: 0.60 < d < 0.84 mm, $\sigma'_v$ = 80 MPa, $e_0$ = 1.12), as shown in Table 1, for which the ratio between the radial deformation and the axial deformation was essentially lower than $10^{-3}$, and in two cases only, in correspondence of the maximum value of the applied $\sigma'_v$, have reached the maximum value of $1.56 \times 10^{-3}$. All these considerations have led to the conclusion that for the tests performed, 1D deformation conditions can be considered and are therefore suitable for the determination of $K_0$.

## 5. Typical Results

In total, 46 tests have been carried out (38 on sand C and 8 on sand Q), as shown in Table 1. All tests have been performed on dry sands in a temperature- and humidity-controlled environment. From the 38 tests performed on C sand, 18 tests were performed with only a cycle of load–unload, while 20 tests were carried out with more cycles of load and unload, some of which with the $\sigma'_{vmax}$ = constant, and some others with increasing $\sigma'_{vmax}$. Tests on quartz sands Q have been carried out with more cycles of load–unload (six with $\sigma'_{vmax}$ = constant and two with increasing $\sigma'_{vmax}$). Principal characteristics and the results of some tests (only 25 tests on 46 for space reasons) carried out are summarised in Table 1. For all the tests, the initial height $h_0$ was equal to 20 mm.

Figure 9 presents typical results of the mean circumferential deformation $\varepsilon_{\theta m}$ in the function of the applied vertical effective stress $\sigma'_v$.

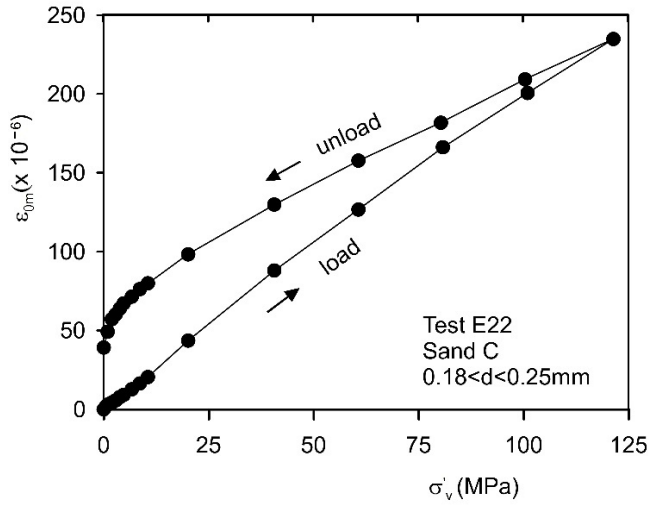


**Figure 9.** Typical results of measured mean circumferential strain $\varepsilon_{\theta m}$ in function of the applied effective vertical stress $\sigma'_v$ for sand C. Note that in the unloaded phase at the end of the test for $\sigma'_v = 0$ the circumferential strain $\varepsilon_{\theta m}$ is greater than zero.

The relation between $\sigma'_h$ and $\sigma'_v$ is reported in Figure 10. Test E8 (sand C) was a test in which only one loading cycle was performed to reach the maximum value of $\sigma'_v$, while tests E12 (sand C) and E13 and E33 (sand Q) were tests in which the maximum value of $\sigma'_v$ was reached through more cycles of load–unload–reload. In the figure the paths of $\sigma'_v$ were reported.

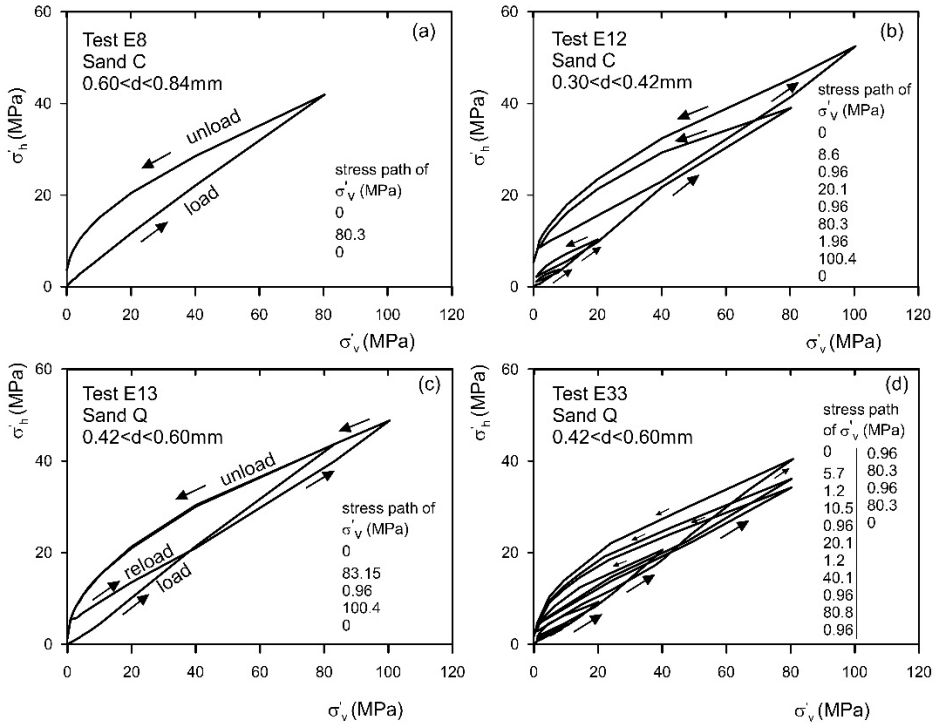


**Figure 10.** Typical results of measured effective horizontal stress $\sigma'_h$ in function of applied effective vertical stress $\sigma'_v$ for sand C (**a**,**b**) and sand Q (**c**,**d**). Note that at the end of the tests $\sigma'_h$ is greater than zero.

In test E33 in correspondence of the maximum value of $\sigma'_v$ (80 MPa), more loading–unloading–reloading cycles have also been carried out. In the load phases, the horizontal stress $\sigma'_h$ increased about linearly, with a vertical stress $\sigma'_v$ of one both for sand C and Q. In the unloading phases, $\sigma'_h$ initially decreased almost linearly with $\sigma'_v$, always for both sand C and Q, until $\sigma'_v$ was about 25–30% of the maximum value that $\sigma'_{v,max}$ reached in the generical load cycle. Subsequently there is a nonlinear relation between $\sigma'_h$ and $\sigma'_v$. The horizontal stress $\sigma'_h$ at the end of the tests was greater than zero; hence, in the specimen, residual radial (horizontal) stresses remained (Figures 9 and 10). Specimens at the end of the test were very strong and resistant and could be extracted whole from the oedometer (Figure 11). These specimens could be assimilated to soft sandstones and could represent the initial phase of the phenomena that occurred in the formation of this type of soft sedimentary rocks. In fact, the reached vertical stress level (up to 100 MPa) represents what occurs in nature at depths of about 4–5 km or more.

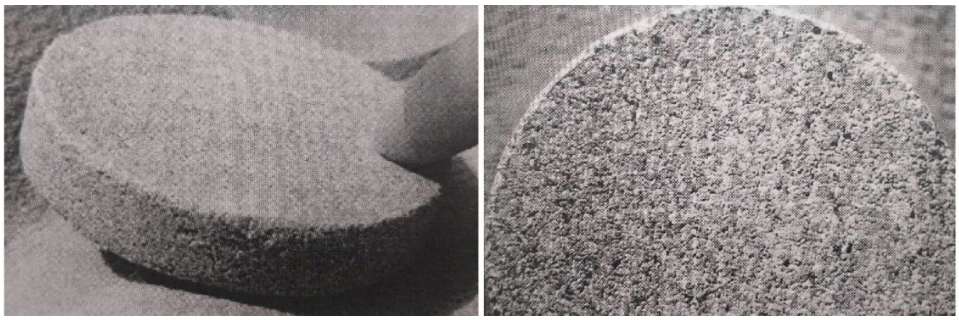

(**a**) (**b**)

**Figure 11.** Specimens of sand C at the end of the test. (**a**) Test 7, initial sand 0.42 mm < d < 0.60 mm; (**b**) test 5, initial sand 0.60 mm < d < 0.84 mm.

A vertical section of the specimen of test 7 is reported in Figure 12. The structure of the sand became extremely dense; it presented a very high degree of interlocking due to the high reduction in porosity linked to the interconnected phenomena of the relative displacements of grains and of the strongly variations of granulometric composition due to the grain-crushing phenomena, both for carbonate and quartz sands. In this configuration, the grain contacts were of concavo-convex type, inter-penetrating, sutured and sigmoidal (like those of locked sands, [61–63]); the coordination number of grains [64,65] was very high, and the soil seemed to possess a sort of apparent cohesion (Figures 11 and 12).

**Figure 12.** Vertical section of specimen 7 of sand C at the end of the test. The final height of the specimen was 13 mm.

The breakage of grains induced a very assorted final grading of sands, as shown in Figure 13. The reduction of the specific volume v (v = 1 + e) could reach values higher than 75% for the C sand 50% for sand Q (Figure 14). Curves presented classical trends with low compressibility at the start of the test until the vertical stress $\sigma'_v$ reached a value of 5–8 MPa for sand C and greater than 15–20 MPa for sand Q. In these ranges of vertical stresses, the deformations were essentially due to the relative displacements of the grains and, to a small extent, to the grain crushing. Subsequently, with the increase of the stress level, the deformations due to breakage of grains became predominant, and the compressibility of the sands increased. From a phenomenological point of view, the volumetric behaviour of sand C and Q was the same, but the high compressibility of sand Q began at values of vertical stress $\sigma'_v$ higher than for sand C. This behaviour was linked to the very different intrinsic strength of the sand particles of the two sands.

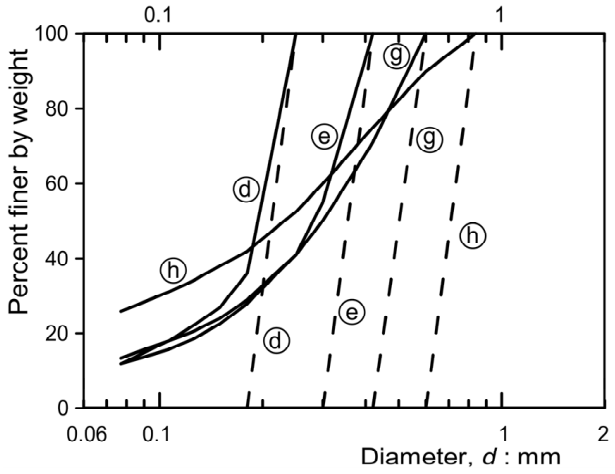


**Figure 13.** Evolution of grain size composition of sand C for $\sigma'_v$ = 80 MPa.

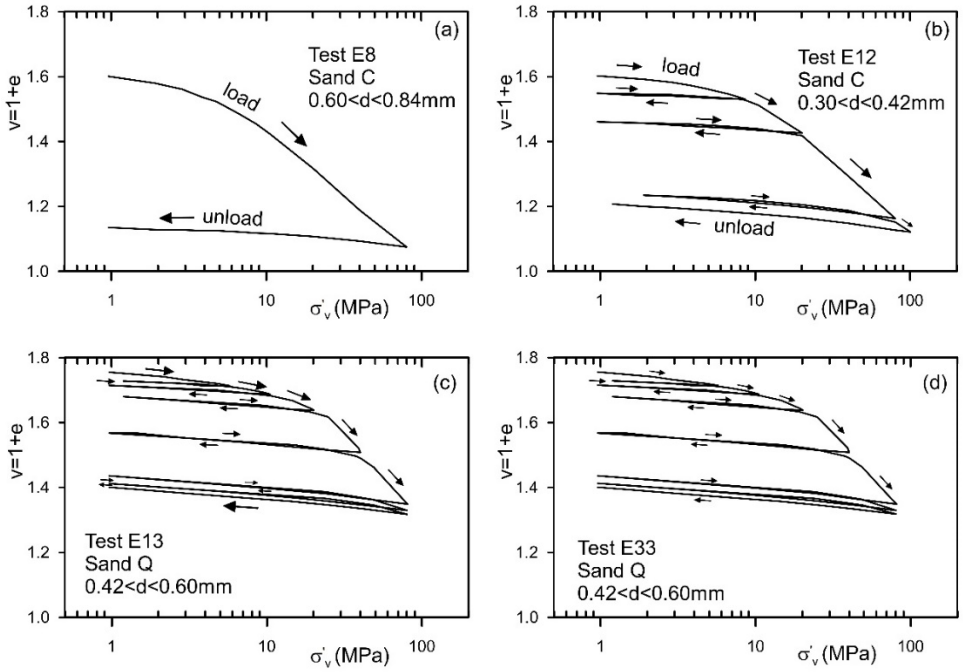


**Figure 14.** Typical results of specific volume $v$ in function of $\sigma'_v$. Sand C (**a**,**b**); sand Q (**c**,**d**); only a cycle of load–unload (**a**,**c**); more cycles of load–unload–reload (**b**,**d**).

Figure 15 shows typical stress paths in the plane s′–t ($s' = 0.5(\sigma'_v + \sigma'_h)$, $t = 0.5(\sigma'_v - \sigma'_h)$). This representation of results determines the value of the parameter β, from which it is possible to determine the parameter ξ, which makes it possible to evaluate $K_0$, as indicated by Daramola (1980) [23], and allows the determination of Poisson's ratio ν′ (Wroth, 1972 and 1975 [8,9]); see Table 1.

In Figure 16, some results of the stress paths in the plane $\ln(p'/p'_{max}) - (q/p')$ (in which $p' = (\sigma'_v + 2\sigma'_h)/3$ was the mean effective stress, and $q = (\sigma'_v - \sigma'_h)$ was the deviatoric stress) are represented. This representation of the results determines the value of the parameter $m$, from which it is possible to determine the value of $K_{0,C}$ for high values of OCR, as indicated by Wroth, 1972 [8].

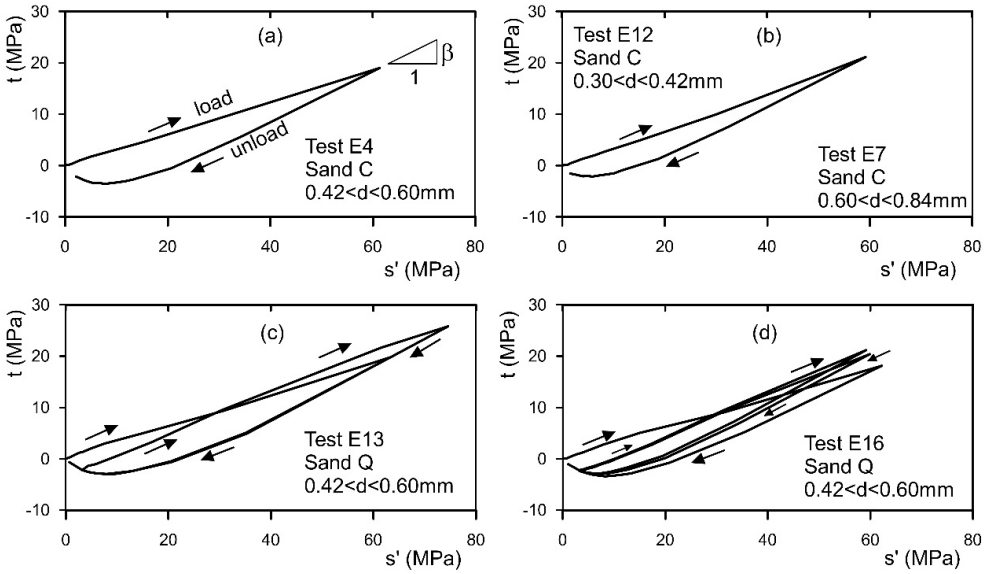


**Figure 15.** Typical results in the plane s′–t ($s' = 0.5(\sigma'_v + \sigma'_h)$; $t = 0.5(\sigma'_v - \sigma'_h)$). Sand C (**a**,**b**); sand Q (**c**,**d**). (Wroth, 1975 [9]).

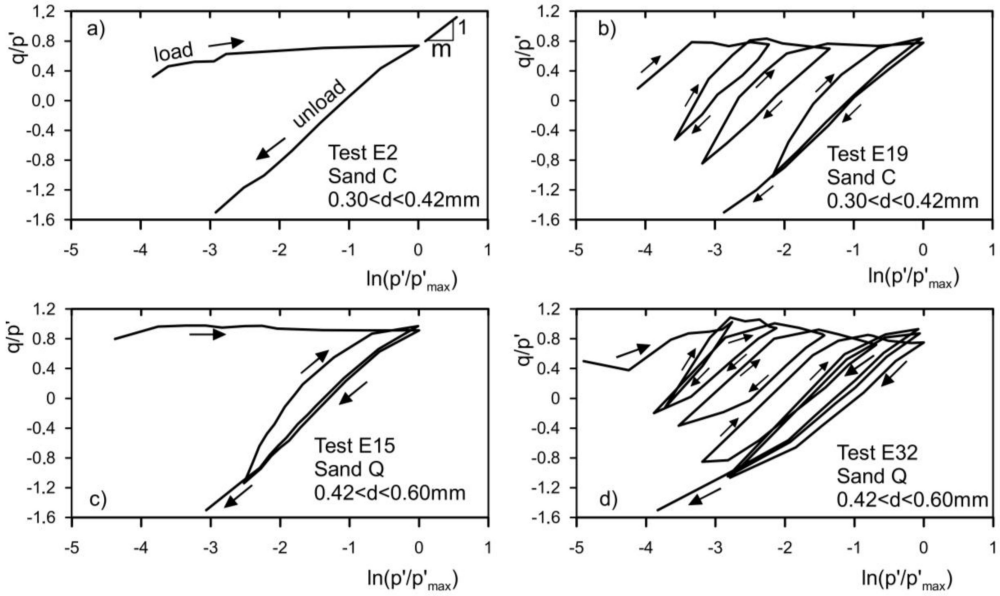


**Figure 16.** Typical results of ratio ($q/p'$) in function of ln ($p'/p'_{max}$). Sand C (**a**,**b**); sand Q (**c**,**d**). (Wroth, 1972 [8]).

## 6. Discussion

### *6.1. Variation of $K_0$ with the Stress Level*

Figure 17 presents some results of the trend of $K_0$ during the tests in the loading and unloading phases. For both sands C and Q, the coefficient $K_0$ was lower than 1 in the phases of the first loading (normal consolidated sands). In the unloading phases, $K_0$ increased with the over-consolidation ratio OCR for both sands C and Q and reached values up to 8–10. It should be noted, however, that for high OCR values, $K_0$ for C sands was higher than those of Q sands. This was due to the greater variations that occurred in the structure of the sands linked to the grain crushing phenomenon which, at the same stress level reached, was more intense in sand C. The described trend was independent by the initial state of the sands (mineralogic composition, grading and initial void ratio).

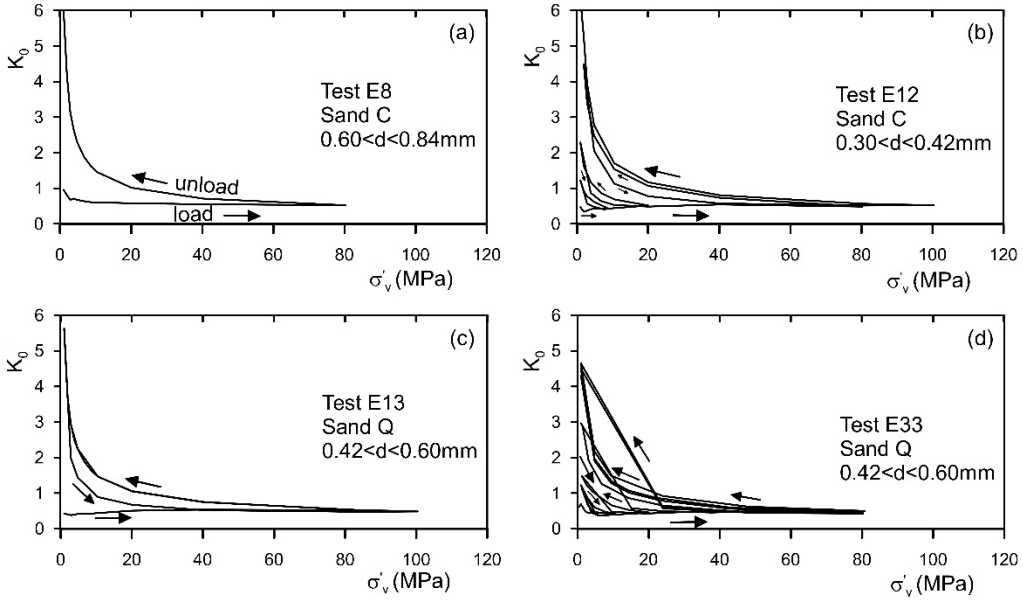


**Figure 17.** Typical trends of coefficient $K_0$ in function of applied $\sigma'_v$ for sand C (**a**,**b**) and for sand Q (**c**,**d**).

### *6.2. Normal Consolidated Sands*

Figure 18 presents the results of the trend of $K_{0n}$ relative to the loading phase only (normal consolidated sands). For both sands C and Q, the coefficient $K_{0n}$ was always lower than 1 in the phases of first loading and up to very high applied vertical stress $\sigma'_v$. In the first part of the loading phases, for $\sigma'_v$ ranging from about 0.2 to 4 MPa, the mean value of $K_{0n}$ decreased from values of 0.9 to values of 0.49 for the calcareous sand C and from 0.8 to 0.45 for quartz sand Q. However, in this range of $\sigma'_v$, there was a maximum dispersion of data, and there was the maximum deviation around the mean value equal to 0.08 for sand C and 0.06 for sand Q in correspondence of $\sigma'_v$ = 4 MPa. This deviation of data is linked to the phenomenon of breakage of particles that, in this range of $\sigma'_v$, is very intense specially for sand C, and is different for the different sands in function of their initial mineralogic and granulometric composition and shape of the particles. For $\sigma'_v$ greater than 4 MPa, the mean value of $K_{0n}$ was 0.52 for sand C and 0.51 for sand Q. The deviation around the mean values decreased with the increases of $\sigma'_v$, and for $\sigma'_v$ greater than 25 MPa for sand C and 40 MPa for sand Q, the deviation was smaller than 0.04 for sand Q and 0.05 for sand Q.

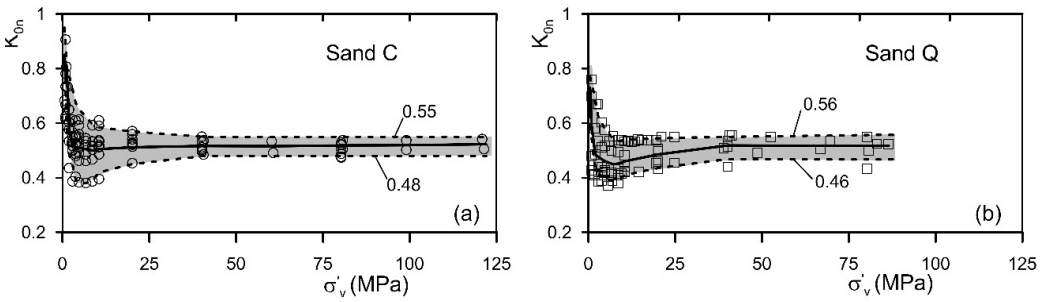


**Figure 18.** Trend of coefficient $K_{0n}$ with applied $\sigma'_v$ for sand C (**a**) and for sand Q (**b**) in the loading phase (normal consolidated sands).

The trend described was observed for both calcareous and quartz sand, although for the Q sand, the changes were negligible starting from $\sigma'_v$ higher than that of the C sand. These variations of $K_{0n}$ depended on the high variation of the structure of the sands linked to the breakage of the particles, the intensity of which varied non-continuously but intermittently and, in some cases, abruptly. The changes of the structure of the sand, linked to the grain crushing and to the reduction of porosity due both to the relative displacements and to the same grain crushing, was not a continuous process but a succession of relatively stable configurations in which equilibrium between the applied stress $\sigma'_v$ and the intergranular stresses existed. An increase of $\sigma'_v$ induced an increasing of the intergranular forces, some breakage of grains and changes of the structure of the sand and, subsequently, variations of the value of $K_{0,n}$. Because of the changes of the structure of the sands described above, for $\sigma'_v$ greater than about 2 MPa, the values of $K_{0n}$ were independent of the initial void ratio. The values of $K_{0n}^{(1)}$, $K_{0n}^{(2)}$ and $K_{0n}^{(*)}$ for $\sigma'_v$ = 0.96 MPa and 1.96 MPa and the value of $\sigma'_{vmax}$ reached in the test are reported in Table 1. Similar trends of $K_{0n}$ have been observed by Yamamuro (1993) [27] and Bopp (1994) [28] for the quartz sand and for the Cambria sand (a sand made by grains of medium strength and hardness). These authors have reported values of $K_{0n}$ that decreased from 0.8 to 0.4 for $\sigma'_v$ ranging from 1 MPa to 10 MPa. The reduction of $K_{0n}$ with the vertical applied stress $\sigma'_v$ has been reported in other papers [57,66] for quartz sand in the field of low mean stress levels. The surprisingly high values of $K_{0n}$ in the low stress range for medium-dense sands of different nature and mineralogical constitution, such as sands C and Q, characterised by values of the shear strength angle greater than 40°, are clearly in disagreement with Jaky's relationship, which would lead to very low values of $K_{0n}$. These results must be related to the confectioning technique by tamping of the specimens, as observed by Terzaghi and Peck (1948, [67]): "…$K_0$ is an empirical constant known as the *coefficient of earth pressure at rest*. Its value depends on the relative density of the sand and the process by which

the deposit was formed. If this process did not involve artificial compaction by tamping, the value of $K_0$ ranges from about 0.4 for loose sand to 0.5 for dense sand. Tamping in layers may increase the value to about 0.8. . .". Similar conclusions have also been reported by other authors [34,68–71] for quartz sands. For calcareous sand, a value of 0.57 was reported by Coop and Lee (1993) [72]. In all the data of these studies, the value of $K_{0n}$ was higher than that predicted by Jaky's relation. For $\sigma'_v$ higher than about 15–20 MPa and up to 120 MPa, the coefficient $K_{0n}$ was subjected to very low variations for both sands C and Q. This result was very surprising considering that in this high range of stresses, the sands undergo very high reduction of porosity and deep changes of grading, tessiture and structure. In the field of low mean stresses sands, C presented peak angles of shear strength $\varphi'_p$ in the range 38–50° depending on relative density, values of $\varphi'_{cv}$ (angle of shear strength at constant volume) in the range 35–37° and values of $\varphi'_r$ (residual angle of shear strength) in the range 32–33° [50]. Dense Q sands at low pressures presented very high peak angles of shear strength $\varphi'_p$, higher than 50° [73]. This last data is reported, along with many other literature data [26,30,50,72,74–81], in Figure 19. Data represented in Figure 19 clearly demonstrate how, at high stress levels, the angle of shear strength was almost constant both for quartz and for carbonate sands and for other sands of different nature and mineralogical constitution.

For p′ ranging from 10 to 700 MPa the angle of shear strength for both C and Q sands is about 32–33°. With this value of the angle φ′, Jaky's relation would provide a value of $K_{0n}$ of 0.46–0.47 that is in very good agreement with the measured values for both sands C and Q. These results demonstrated that Jaky's relation provides good prevision of $K_{0n}$ at medium-high stress if the angle of the shear strength is that relative to the high pressures in which the dilation and the rearrangement components of the shear resistance are nil or negligible. In the field of low-medium stress levels Jacky's relation would provide results in high disagreement with the experimental data if the peak angle of shear strength is considered. A better forecast is made if the constant volume angle of shear strength is considered, in agreement with the relation proposed by Mesri and Hayat (1993) [18], although results reported by these researchers are referred to low-medium stress levels and principally to clayey soils.

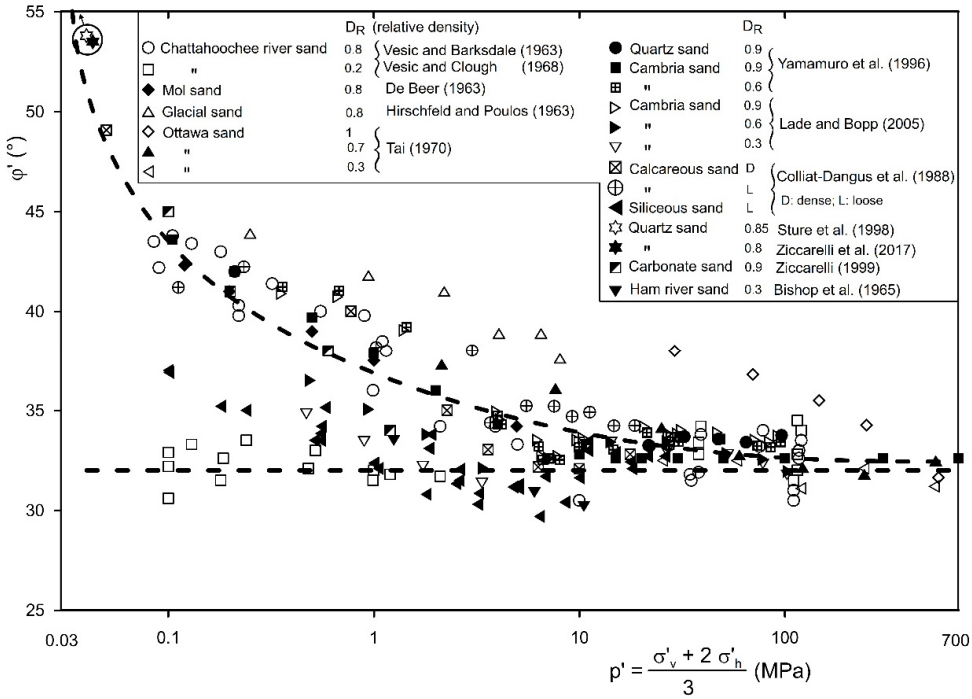


**Figure 19.** Trend of shear strength angle φ′ in the function of mean effective stress p′ for sands of different mineralogical compositions and different initial relative densities, $D_R$.

Obtained results are in disagreement with the relation proposed by Hendron 1963 [17] (which would provide lower values than that of Jacky). A good prediction is obtained with the relation proposed by Federico et al. [19] (although these authors essentially refer to clayey soils and low stress levels) if the constant volume shear strength angle is considered.

Basically, the results obtained in the experimentation allow to state that (at least for carbonate and quartz sands) for mean stress levels higher than a few of MPa, the main existing relationships (i.e., relationships (4), (6), (7) and (8)) provide a good prediction of $K_{0n}$ if this latter is determined with reference to the constant volume angle of shear resistance and not to the peak one.

Based on the experimental results and on the considerations above described, the following relationship is proposed:

$$K_{0n} = 1 - \sin\ \varphi'_{cv} \tag{23}$$

This relationship is similar to the one like that of proposed by Mesri and Hayat (1993) [18] (expression (7), with $\varphi'_{cv}$ instead of $\varphi'$) who however refer to clays and for effective vertical stresses up to 500 kPa.

It should be highlighted that the proposed relationship (23) is valid for both carbonate and siliceous sands, therefore for a very wide range of strength and stiffness of the grains, and is valid up to very high effective vertical stresses (120 MPa), hence for a very high range of stresses (0–120 MPa).

It is worth pointing out that, at least for the sands employed in the texts, $K_{0n}$ is significantly less than one, contrary to what was postulated by Heim (1932) [82], which says that the stress state tends to be isotropic ($K_{0n}$ = 1) at very high depth.

### *6.3. Over-Consolidated Sands*

The coefficient of earth pressure at rest $K_{0C}$ of the over-consolidated sands varies in the unloaded phase in function of the overconsolidation ratio OCR with a relation like that proposed by Schmidt (1966 and 1967) [20,21] and Alpan (1967) [22]:

$$K_{0C} = a(OCR)^b \tag{24}$$

Figure 20 presents the results of 4 tests (2 for C sand and 2 for Q sand). The values of coefficients *a* and *b* are reported in Table 1 for all tests. Coefficient *a* varies from 0.46 to 0.69 for sand C and from 0.48 to 0.57 for sand Q, while coefficient *b* varies from 0.43 to 0.53 for sand C and from 0.47 to 0.57 for sand Q, Figure 21 and Table 1. Coefficient *a* decreases slightly with the increase of the initial void ratio $e_0$ for sand C, while it seems independent by $e_0$ for sand Q. Coefficient *b* seems independent by $e_0$ for both sands C and Q.

Figure 22 (a and b are the subfigure) represents all the data for sand C and Q respectively. Considering all data the coefficient $K_{0C}$ of sand C can be represented by the following relation (data present a very good value of the determination coefficient: $R^2$ = 0.98, Figure 22a):

$$K_{0C} = 0.44(OCR)^{0.61} \tag{25}$$

The values of *a* and *b* that represent the minimum and the maximum trend of $K_{0C}$ are 0.35 and 0.52 (coefficient *a*) and 0.60 and 0.63 (coefficient *b*) respectively.

All data can be described between a minimum value of $K_{0C}$, in which *a* = 0.35 and *b* = 0.6 and a maximum value in which *a* = 0.52 and *b* = 0.63 (Figure 22a).

Q sands can be described by the relation ($R^2$ = 0.97):

$$K_{0C} = 0.43(OCR)^{0.56} \tag{26}$$

For this sand coefficient *a* and *b* corresponding to the minimum and the maximum trend of $K_{0C}$ are 0.37 and 0.51 (coefficient *a*) and 0.55 and 0.56 (coefficient *b*) respectively, Figure 22b. The mean values of coefficients *a* and *b* are very close for the two sands of different nature and mineralogy, initial grading and porosity.

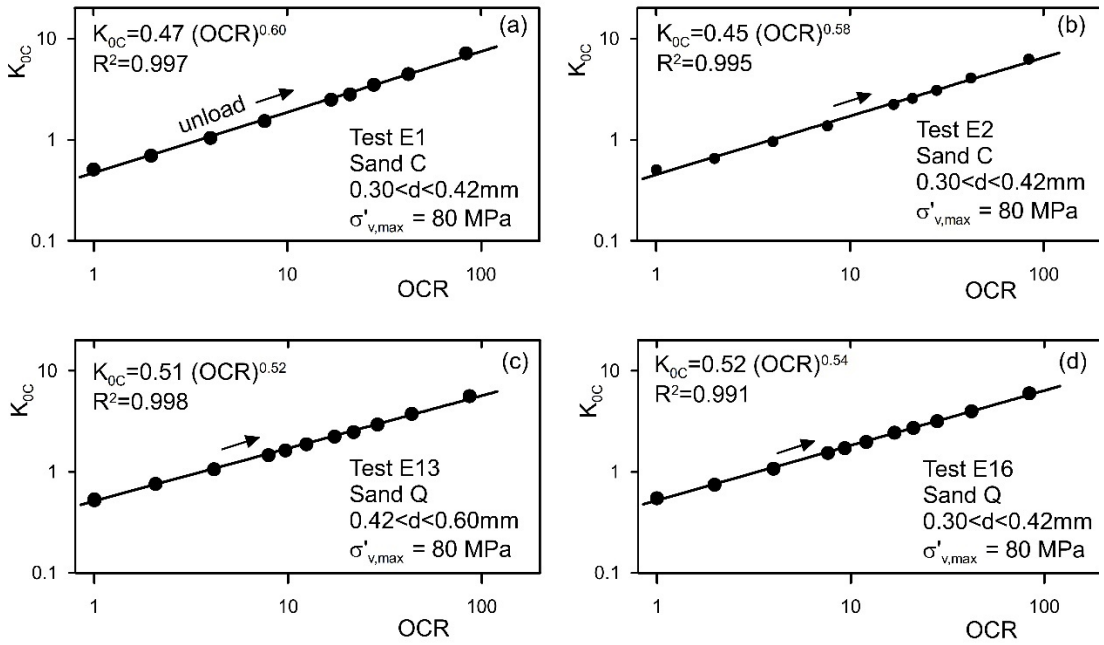


**Figure 20.** Relation between coefficient $K_{0,C}$ and the overconsolidation ratio OCR for sand C (**a**,**b**) and sand Q (**c**,**d**).

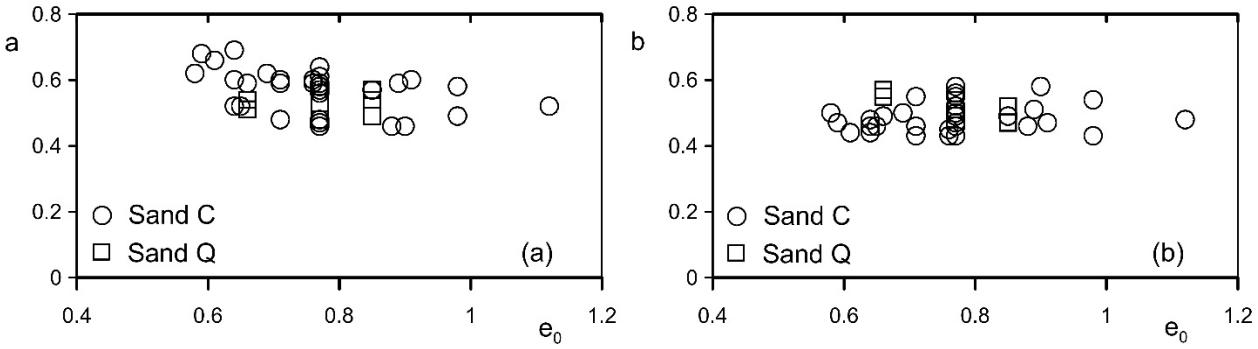


**Figure 21.** Coefficients *a* (**a**) and *b* (**b**) in function of initial void ratio $e_0$ of sands C and Q.

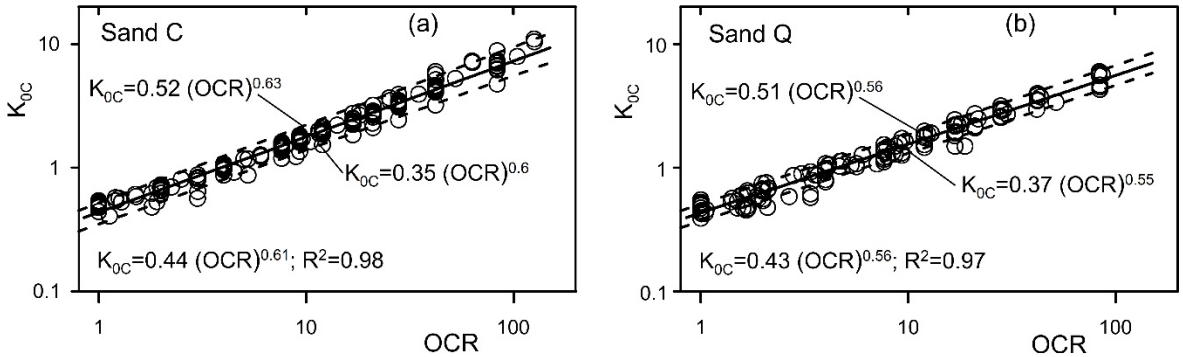


**Figure 22.** Relation between coefficient $K_{0,C}$ and overconsolidation ratio OCR for sand C (**a**) and sand Q (**b**) considering all data.

The mean values of coefficient *a* are in good agreement with the relation of Mayne and Kulhawy (1982) [10] always if the constant volume shear strength angle is considered for the determination of coefficient *a* and the shear strength angle at high pressures is used

for determination of coefficient *b*. It should be noted, however, that Mayne and Kulhawy's results refer to maximum OCR essentially lower than 30.

The relationship proposed by Daramola, 1980 [23] also provides a good prediction if the relative coefficient of earth pressure at rest $K_{0n}$ is determined considering the critical state angle of shear resistance $\varphi'_{cv}$ and a medium value of coefficient ξ, (Figure 23 and Table 1) is considered. Analogues consideration can be do for the relation of Parry (2004) [25], the which is in good agreement with the experimental data of the present research, if, for the determination of the coefficient of the Parry's expression, the angle of shear resistance at high pressure (or that corresponding to the ultimate state at the low-medium pressures $\varphi'_{cv}$) is considered.

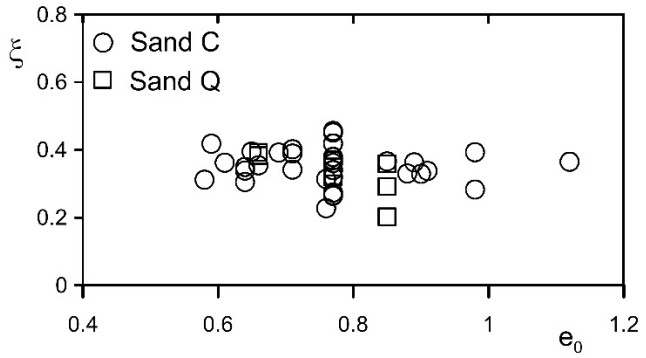


**Figure 23.** Trend of coefficient ξ, (Daramola, 1980 [23]) with the initial void ratio $e_0$ for sands C and Q.

The relationships proposed by Wroth (1972 and 1975) [8,9] also provide a good prediction for both slightly over-consolidated soils (OCR < 5) and heavily over-consolidated soils (OCR > 5) respectively, always if $K_{0n}$ is determined considering the angle of shear strength corresponding to the ultimate state or that corresponding to very high pressures.

Finally, even the main relationships relative to the over-consolidated soils (i.e., relationships (9), (10), (11), (12), (13) and (16)) provide a good prediction of $K_{0C}$ if in the different formulas the various coefficients are calculated with reference to the critical state angle of shear strength and not to the peak one. Figure 24 reports the trends of ν′ and *m* [8,9] in function of the initial void ratio $e_0$ are reported. The value of ν′ varies between about 0.2 and 0.3 and is independent of $e_0$, for coefficient m there is a tendency to increase in function of $e_0$ although much dispersion is present for both sands C and Q. Coefficient *m* varies in the range 1.05–1.5 for both C and Q sands.

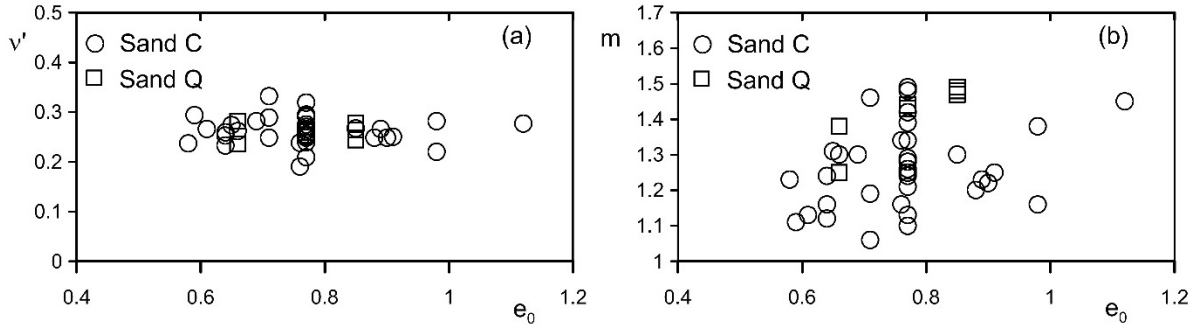


**Figure 24.** Trend of coefficients ν′ (**a**) and *m* (**b**) (Wroth, 1975 [9]) with the initial void ratio $e_0$ for sands C and Q.

On the basis of the experimental results and of the observations described above, is proposed the following relation:

$$K_{0C} = K_{0n}(OCR)^{\sin\ \varphi'_{cv}} \quad (27)$$

where

$$K_{0n} = (1 - \sin \varphi'_{cv})$$

The relationship (27) is similar to the one proposed by Mayne and Kulhawy (1982) [10] but with the constant volume angle of shear resistance $\varphi'_{cv}$ instead of the peak one $\varphi'$ and similar to the relation proposed by Terzaghi et al. (1996) [24]). Furthermore, the relationships proposed by these researchers refer to medium-low stress levels and maximum OCR values of 30.

The proposed expression (27) is valid for both calcareous and quartz sands (therefore for a very wide range of stiffness and strength of the sand particles), for values of OCR up to 120, hence for both for slightly and heavily over-consolidated sands and up to very high stresses (120 MPa).

The results above described probably are linked to the strong evolution of grading and to the high variation of structure of the sands due to the grain crushing phenomenon. It should be noted that for high values of OCR coefficient $K_{0C}$ is greater than Rankine's passive coefficient of earth pressure $K_p$ even if the latter is calculated in reference to the peak angle of the shear strength at low pressures in which the dilation component of the shear strength is relevant. This result is due to the very locked structure of the sands owing to the breakage of grains, with intergranular contact of sutured and sigmoidal, concavo-convex type, inter penetrating, that confer to the sand a sort of apparent cohesion, see Figures 11 and 12. This very dense structure explains the reasons because $K_{0C}$ can be greater than $K_p$, which, for normal soils and at medium-low stress levels, represents an upper limit of $K_{0C}$, Terzaghi et al. (1996) [24].

Finally, it should be underlined that the results of the conducted research have great practical relevance for very special and important geotechnical problems, such as very high earth dams, deep excavation support structures, deep mine shafts, deep tunnels and deep well shafts for the storage of nuclear waste, soils under the tip of deep driven foundation piles, explosions, projectile impacts and also in some geological and geophysical problems. In all these cases, very high stress levels occur and for the study of soil behavior, soil-structure interaction and for the design of structures, knowledge of the earth pressure coefficient at rest $K_0$ (referred to these very high stress levels and high values of OCR) is necessary, both for normalconsolidated and over-consolidated soils.

## 7. Conclusions

The results of a very extensive experimental investigation on the coefficient of earth pressure at rest $K_0$ of sands up to very high effective vertical stresses are reported and discussed in the paper.

For normal consolidated sands, the coefficient $K_{0n}$ depended on the stress level. In the loading phase, $K_{0n}$ decreased with the vertical effective stress $\sigma'_v$. It passed from values of about 0.9 to values of about 0.45 in the range of $\sigma'_v$ between about 0.2 MPa and 4 MPa. Subsequently, $K_{0n}$ was about constant, and the mean values were about 0.5 for both sand C and Q, until very high vertical effective stresses (120 MPa). In the range of $\sigma'_v$ = 4–10 MPa, there were small variations linked to the high modifications of the structure of the sands due to the grain-crushing phenomenon. The latter was very intense for both sands, although for sand C, it started at stress levels lower than those of sand Q. The deep modifications of texture and structure of the sand, due to the breakage of grains in the initial phase of load (up to 8–10 MPa), imply that $K_{0n}$ at higher stress levels was almost constant for both sands C and Q, with values in the range 0.45–0.55.

These results do not confirm Heim's conjecture (at least for the tested sands), according to which the stress state at great depths should become uniform and therefore $K_{0,n}$ should tend to the value one.

For the tested sands, the mean existing relationships, including the well-known and utilized Jaky's relation, did not lead to reliable results at relatively low stress levels (probably due to the modality the specimens were packaged, which occurred by gently tamping) if the peak angle of shear strength was employed. A good prediction was obtained if the constant

angle of shear strength $\varphi'_{cv}$ was used. At high stress levels, the principal relationships of literature and reported in the paper provide a good prediction if the corresponding angle of shear strength at high pressures is used.

For the over-consolidated sands, the relationship between $K_{0C}$ and OCR is describable through a relationship $K_{0C} = a\ (OCR)^b$ as proposed by Schmidt (1967 [21]), with mean values of coefficient $a$ equal to 0.44 for sand C and 0.37 for sand Q and coefficient $b$ equal to 0.61 for sand C and 0.56 for sand Q. Even the others principal relationships present in the literature relative to the over-consolidated soils provide a good prediction both for low and high OCR values if the coefficients present in them were calculated with reference to the constant volume angle of shear strength. In the tests with more cycles of load–unload–reload, with increasing maximum vertical stress reached in the single load cycle, in the cycles of unload, the $K_{0C}$ varied with the predicted relation. In the phases of reloading, when the maximum value of the vertical stress previously reached in the loading phase (OCR = 1) was reached again, the coefficient $K_{0C}$ reached the value previously achieved in the previously loaded phase.

For values of $\sigma'_{vmax}$ about 35–40 MPa, the sands were very dense, and they were similar to weak sandstone because of the strong modifications of the structure, texture and type of grain contacts, linked to the particle's breakage. This condition explains the measured values $K_{0C}$ greater than Rankine's passive earth pressure coefficient $K_p$

Finally, the following expressions are proposed.

- For normally consolidated sands (valid for $\sigma'_v$ up to 120 MPa): $K_{0n} = 1 - sin\varphi'_{cv}$.
- For over-consolidated sands valid for OCR up to 120 and $\sigma'_v$ up to 120 MPa: $K_{0C} = K_{0n}\ (OCR)^{sin\varphi'_{cv}}$.

**Funding:** This study received no external funding.

**Data Availability Statement:** Data are available upon request.

**Conflicts of Interest:** The author declares no conflicts of interest.

## References

1. Jardine, R.J.; Symes, M.J.; Burland, J.B. The measurement of soil stiffness in the triaxial apparatus. *Géotechnique* **1984**, *3*, 323–340. [CrossRef]
2. Jardine, R.J.; Potts, D.M.; Fourie, A.B.; Burland, J.B. Studies on the influence of non-linear stress-strain characteristics in soil-structure interaction. *Géotechnique* **1986**, *36*, 377–396. [CrossRef]
3. Atkinson, J.H. Non-linear soil stiffness in routine design. *Géotechnique* **2000**, *50*, 487–508. [CrossRef]
4. Wang, L.; Shi, W.; Zhou, Y. Adaptive-passive tuned mass damper for structural aseismic protection including soil–structure interaction. *Soil. Dyn. Earthq. Eng.* **2022**, *158*, 107298. [CrossRef]
5. Xu, H.; Cai, X.; Wang, H.; Li, S.; Huang, X.; Zhang, S. Analysis of the working response mechanism of wrapped face reinforced soil retaining wall under strong vibration. *Sustainability* **2022**, *14*, 9741. [CrossRef]
6. Brooker, E.W.; Ireland, H.O. Earth Pressures at rest related to stress history. *Can. Geotech. J.* **1965**, *2*, 1–15. [CrossRef]
7. Mitchell, J.K.; Soga, K. *Fundamentals of Soil Behavior*, 3rd ed.; John Wiley & Sons: New York, NY, USA, 2005; ISBN 978-0-471-46302-3.
8. Wroth, C.P. General theories of earth pressures and deformations. *Proc. Eur. Conf. Soil Mech.* **1972**, *2*, 33–52.
9. Wroth, C.P. In situ measurement of initial stresses and deformation characteristics. In *Conference on In Situ Measurement of Soil Properties*; ASCE: New York, NY, USA, 1975; Volume 2, pp. 181–227.
10. Mayne, P.W.; Kulhawy, F.H. K0-OCR relationship in soil. *ASCE J. Geotech. Eng. Div.* **1982**, *108*, 851–872. [CrossRef]
11. Jefferies, M.G.; Crooks, J.H.A.; Becker, D.E.; Hill, P.R. Independence of geostatic stress from overconsolidation in some Beaufort Sea clays. *Can. Geotech. J.* **1987**, *24*, 342–356. [CrossRef]
12. Amadei, B.; Stephansson, O. *Rock Stress and Its Measurement*; Chapmann & Hall: London, UK, 1997; ISBN 978-94-010-6247-3.
13. Schnaid, F.; Odebrecht, E.; Sosnoski, J.; Robertson, P.K. Effects of test procedure on flat dilatometer test (DMT) results in intermediate soils. *Can. Geotec. J.* **2016**, *53*, 1270–1280. [CrossRef]
14. Chen, C.L.; Jia, Y.J.; Jin, J.; Zhang, D.F.; Sun, Y.R.; Li, F.L. Influences of water content and stress on coefficient of lateral pressure at rest of undisturbed loess. *Chin. J. Rock Mech. Eng.* **2017**, *36*, 3535–3542. [CrossRef]
15. Jaky, J. *A Magyar Mérnök-és épitész-Egylet Közlönye*; 1944; Volume 78, pp. 355–358. Available online: https://repozitorium.omikk.bme.hu/items/ee5fd5fe-48a3-49da-a6a5-573e267ed01d (accessed on 15 September 2024).

16. Jaky, J. Pressure in silos. In Proceedings of the Second International Conference on Soil Mechanics and Foundation Engineering, Rotterdam, The Netherlands, 21–30 June 1948; University of London Northampton Square: London, UK, 1948; Volume 1, pp. 103–107.
17. Hendron, A.J. The Behavior of Sand in One-Dimensional Compression. Ph.D. Thesis, University of Illinois at Urbana, Champaign, IL, USA, 1963.
18. Mesri, G.J.; Hayat, T.M. The coefficient of earth pressure at rest. *Can. Geotech. J.* **1993**, *30*, 647–666. [CrossRef]
19. Federico, A.; Elia, G.; Germano, V. A short note on the earth pressure and mobilized angle of internal friction in one-dimensional compression of soils. *J. Geoeng.* **2008**, *3*, 41–46. [CrossRef]
20. Schmidt, B. Earth pressure at rest related to stress history: Discussion. *Can. Geotech. J.* **1966**, *3*, 239–242. [CrossRef]
21. Schmidt, B. Lateral Stresses in Uniaxial Strain. In *Geoteknisk Institute*; Bulletin; The Danish Geotechnical Institute: Copenhagen, Denmark, 1967; pp. 5–12.
22. Alpan, I. The empirical evaluation of the coefficient $K_0$ and $K_{0R}$. *Soil Found* **1967**, *7*, 31–40. [CrossRef]
23. Daramola, O. On estimating $K_0$ for overconsolidated granular soils. *Géotechnique* **1980**, *30*, 310–313. [CrossRef]
24. Terzaghi, K.; Peck, R.B.; Mesri, G. *Soil Mechanics in Engineering Practice*, 2nd ed.; John Wiley: New York, NY, USA, 1996; ISBN 0471086584.
25. Parry, R.H.G. *Mohr Circles, Stress Paths and Geotechnics*, 2nd ed.; CRC Press: Boca Raton, FL, USA; Taylor & Francis Group: London, UK, 2004; ISBN 9780367871253.
26. Tai, T.L. Strength and Deformation Characteristics of Cohesionless Materials at High Pressures. Ph.D. Dissertation, Department of Civil & Environmental Engineering, Durham, NC, USA, 1970.
27. Yamamuro, J.A. Instability and Behaviour of Granular Materials at High Pressures. Ph.D. Dissertation, UCLA Civil and Environmental Engineering, Los Angeles, CA, USA, 1993.
28. Bopp, P.A. Effect of Initial Relative Density on Instability and Behaviour of Granular Materials at High Pressures. Ph.D. Dissertation, UC Berkeley Civil and Environmental Engineering, Los Angeles, CA, USA, 1994.
29. Hamouche, K.K.; Leroueil, S.; Roy, M.; Lutenegger, A.J. In situ evaluation of $K_0$ in eastern Canada clays. *Can. Geotech. J.* **1995**, *32*, 677–688. [CrossRef]
30. Yamamuro, J.A.; Bopp, P.A.; Lade, P.V. One-dimensional compression of sands at high pressures. *J. Geotech. Eng.* **1996**, *1228*, 147–154. [CrossRef]
31. Gaudin, C.; Schnaid, F.; Garnier, J. Sand characterization by combined centrifuge and laboratory tests. *Int. J. Phys. Model Geotech.* **2005**, *5*, 42–56. [CrossRef]
32. Michalowski, R.L. Coefficient of Earth Pressure at Rest. *J. Geotech. Geoenv. Eng.* **2005**, *131*, 1429–1433. [CrossRef]
33. Northcutt, S.; Wijewickreme, D. Effect of particle fabric on the coefficient of lateral earth pressure observed during one-dimensional compression of sand. *Can. Geotech. J.* **2013**, *50*, 457–466. [CrossRef]
34. Cai, Z.Y.; Dai, Z.Y.; Xu, G.M.; Ren, G.F. Effect of particle size and compaction on $K_0$ value of sand by centrifugal model test. *Rock Soil Mech.* **2020**, *41*, 3882–3888.
35. Chen, S.F.; Kong, L.W.; Luo, T. Lateral stress release characteristics of over-consolidated silty clay and calculation method for lateral earth pressure coefficient at rest. *Rock Soil Mech.* **2022**, *43*, 160–168. [CrossRef]
36. Lee, K.; Kim, J.; Woo, S.I. Analysis of horizontal earth pressure acting on box culverts through centrifuge model test. *Appl. Sci.* **2022**, *12*, 1993. [CrossRef]
37. Li, L.; Dai, Z.; Liu, R.; Jian, F. Experimental study on the coefficient of earth pressure at rest for sand. *Buildings* **2023**, *13*, 1276. [CrossRef]
38. Murphy, D.J. Stress, degradation, and shear strength of granular material. In *Geotechnical Modeling and Applications*; Sayed, S.M., Ed.; Gulf Publishing Co.: Houston, TX, USA, 1987; pp. 181–211.
39. Terzaghi, K. Old earth pressure theories and new test results. *Eng. News Rec.* **1920**, *85*, 632–637.
40. Huntington, W.C. *Earth Pressures and Retaining Walls*; John Wiley & Sons: New York, NY, USA, 1957.
41. Bishop, A.W.; Henkel, D.J. *The Measurement of Soil Properties in the Triaxial Test*, 2nd ed.; E. Arnold & Sons: London, UK, 1962.
42. Bishop, A.W.; Webb, D.L.; Skinner, A.E. Triaxial Tests on Soil at Elevated Cell Pressures. In Proceedings of the 6th International Conference on Soil Mechanics and Foundation Engineering, Montreal, QC, Canada, 8–15 September 1965; University of London: London, UK, 1965; Volume 1, pp. 170–174.
43. Andrawes, K.Z.; El-Sohby, M.A. Factors affecting coefficient of earth pressure $K_0$. *J. Soil Mech. Found Div.* **1973**, *99*, 527–539. [CrossRef]
44. Lambe, T.W.; Whitman, R.V. *Soil Mechanics*; John Wiley: New York, NY, USA, 1979; ISBN 0-471-02261-6.
45. Castellanza, R.; Nova, R. Oedometric tests on artificially weathered carbonatic soft rocks. *J. Geotech. Geoenv. Eng.* **2004**, *130*, 728–739. [CrossRef]
46. Hetényi, M. *Beams on Elastic Foundation*; The Univ of Michigan Press: Ann Arbor, MI, USA, 1946.
47. Timoshenko, S.P.; Woinowsky-Krieger, S. *Theory of Plates and Shells*, 2nd ed.; McGraw-Hill: New York, NY, USA, 1959.
48. Muskhelishvili, N.I. *Some Basic Problems of the Mathematical Theory of Elasticity*; Noordhoff Ltd.: Groninghen, The Netherlands, 1963.
49. Timoshenko, S.P.; Godier, J.N. *Theory of Elasticity*, 3rd ed.; McGraw-Hill: New York, NY, USA, 1970.

50. Ziccarelli, M. Comportamento Meccanico di Sabbie Carbonatiche Bioclastiche in stato di Deformazione Monodimensionale. Ph.D. Thesis, Dottorato di Ricerca in Ingegneria Geotecnica—Consorzio tra le Università di Catania e di Palermo, Catania, Italy, 1999. (In Italian).
51. Terzaghi, K. Large Retaining-Wall Test. In *Engineering News Record*; McGraw-Hill: New York, NY, USA, 1 February 1934; Incorporated Volume 102, N. 20, pp. 136–140. ISSN 0891-9526.
52. Rowe, P.W. General Report on Papers in Section, I. *Proc. Bruss. Conf. Earth Press. Probl.* **1958**, *3*, 25–30.
53. Okochi, K.; Tatsuoka, F. Some factors affecting $K_0$-value of sand measured in triaxial cell. *Soils Found.* **1984**, *24*, 52–68. [CrossRef]
54. Lade, P.V.; Yamamuro, J.A.; Bopp, P.A. Significance of Particle Crushing in Granular Materials. *J. Geotech. Eng.* **1996**, *122*, 309–316. [CrossRef]
55. Chu, J.; Gan, C.L. Effect of void ratio on $K_0$ of loose sand. *Géotechnique* **2004**, *54*, 285–288. [CrossRef]
56. Wanatowski, D.; Chu, J. $K_0$ of sand measured by a plane-strain apparatus. *Can. Geotech. J.* **2007**, *44*, 1006–1012. [CrossRef]
57. Lo, S.-C.R.; Chu, J. The measurement of $K_0$ by triaxial strain path testing. *Soils Found.* **1991**, *31*, 181–187. [CrossRef] [PubMed]
58. Cardona, A.; Bhandari, A.R.; Heidari, M.; Flemings, P.B. The viscoplastic behavior of natural hydrate-bearing sandy-silts under uniaxial strain compression ($K_0$ loading). *J. Geophys. Res. Solid Earth* **2023**, *128*, e2023JB026976. [CrossRef]
59. Park, J.; Santamarina, J.C. Sands Subjected to Repetitive Loading Cycles and Associated Granular Degradation. *J. Geotech. Geoenv. Eng.* **2023**, *149*, 04023111. [CrossRef]
60. Lirer, S.; Flora, A.; Nicotera, M.V. Some remarks on the coefficient of earth pressure at rest. *Acta Geotech.* **2011**, *6*, 1–12. [CrossRef]
61. Dusseault, M.B.; Morgenstern, N.R. Shear strength of Athabasca Oil Sands. *Can. Geotech. J.* **1978**, *15*, 216–238. [CrossRef]
62. Dusseault, M.B.; Morgenstern, N.R. Locked sands. *Q. J. Eng. Geol.* **1979**, *12*, 117–131. [CrossRef]
63. Celauro, C.; Ziccarelli, M.; Parla, G.; Valore, C. An automated procedure for computing the packing properties of dense and locked sands by image analysis of thin sections. *Granul. Matter* **2014**, *16*, 867–880. [CrossRef]
64. Oda, M. Co-ordination number and its relation to shear strength of granular material. *Soils Found.* **1977**, *17*, 29–42. [CrossRef] [PubMed]
65. Ziccarelli, M.; Valore, C. Hydraulic conductivity and strength of pervious concrete for deep trench drains. *Geomech. Energy Environ.* **2019**, *18*, 41–55. [CrossRef]
66. Wanatowski, D.; Chu, J.; Gan, C.L. Compressibility of Changi sand in $K_0$ consolidation. *Geomech. Eng.* **2009**, *1*, 241–257. [CrossRef]
67. Terzaghi, K.; Peck, R.B. *Soil Mechanics in Engineering Practice*, 1st ed.; John Wiley and Sons: New York, NY, USA, 1948; pp. 57–61.
68. Broms, B.; Ingelson, I. Earth pressures against abutments of a rigid frame bridge. *Géotechnique* **1971**, *21*, 15–28. [CrossRef]
69. Duncan, J.M.; Seed, R.B. Compaction-Induced Earth Pressures Under $K_0$-Conditions. *J. Geotech. Eng.* **1986**, *112*, 1–22. [CrossRef]
70. Duncan, J.M.; Williams, G.W.; Sehn, A.L.; Seed, R.B. Estimation earth pressures due to compaction. *J. Geotech. Eng.* **1991**, *117*, 1833–1847. [CrossRef]
71. Hayashi, H.; Yamazoe, N.; Mitachi, T.; Tanaka, H.; Nishimoto, S. Coefficient of earth pressure at rest for normally and overconsolidated peat ground in Hokkaido area. *Soils Found.* **2012**, *52*, 299–311. [CrossRef]
72. Coop, M.; Lee, I.K. The behaviour of granular soils at elevated stresses. In *Predictive Soil Mechanics*; Houlsby and Schofield—Thomas Telford: London, UK, 1993; pp. 186–198.
73. Ziccarelli, M.; Valore, C.; Muscolino, S.R.; Fioravante, V. Centrifuge tests on strip footings on sand with a weak layer. *Geotech. Res.* **2017**, *4*, 47–64. [CrossRef]
74. De Beer, E.E. The scale effect in the transposition of the results of deep-sounding tests on the ultimate bearing capacity of piles and caisson foundations. *Géotechnique* **1963**, *13*, 39–75. [CrossRef]
75. Hirschfeld, R.C.; Poulos, S.J. High-Pressure Triaxial Tests on a Compacted Sand and an Undisturbed Silt. In *Laboratory Shear Testing of Soils*; ASTM International: West Conshohocken, PA, USA, 1963; STP 361; pp. 329–340. [CrossRef]
76. Vesic, A.S.; Barksdale, R.D. On Shear Strength of Sand at Very High Pressures. In *Laboratory Shear Testing of Soils*; ASTM Special Technical Publication: West Conshohocken, PA, USA, 1963; Volume 361, pp. 301–305.
77. Bishop, A.W. Test requirements for measuring the coefficient of earth pressure at rest. *Proc. Bruss. Conf. Earth Press. Probl.* **1958**, *1*, 2–14.
78. Vesic, A.S.; Clough, G.W. Behavior of Granular Granular Material Under High Stress. *J. Soil Mech Found Div.* **1968**, *94*, 661–668. [CrossRef]
79. Colliat-Dangus, J.L.; Desrues, J.; Foray, P. Triaxial Testing of Granular Soil Under Elevated Cell Pressure. In *Advanced Triaxial Testing of Soil and Rock*; ASTM International: West Conshohocken, PA, USA, 1988; pp. 290–310.
80. Sture, S.; Costes, N.C.; Batiste, S.N.; Lankton, M.R.; AlShibli, K.A.; Jeremic, B.; Swanson, R.A.; Frank, M. Mechanics of granular materials at very low effective stresses. *J. Aerosp. Eng.* **1998**, *11*, 67–72. [CrossRef]
81. Lade, P.V.; Bopp, P.A. Relative density effects on drained sand behavior at high pressures. *Soils Found.* **2005**, *45*, 1–13. [CrossRef]
82. Heim, A. *Bergsturz und Menschenleben*; Fretz Wasmuth Verlag: Zurich, Switzerland, 1932; p. 227.